Journal of Computational Physics 323 (2016) 95–114

Contents lists available at ScienceDirect

Journal of Computational Physics

www.elsevier.com/locate/jcp

A conservative semi-Lagrangian HWENO method for the Vlasov equation ☆

Xiaofeng Cai [a], Jianxian Qiu [b], Jing-Mei Qiu [c,*]

[a] School of Mathematical Sciences, Xiamen University, Xiamen, Fujian, 361005, PR China
[b] School of Mathematical Sciences and Fujian Provincial Key Laboratory of Mathematical Modeling & High-Performance Scientific Computing, Xiamen University, Xiamen, Fujian, 361005, PR China
[c] Department of Mathematics, University of Houston, Houston, 77204, United States

ARTICLE INFO

Article history:
Received 1 January 2016
Received in revised form 14 June 2016
Accepted 20 July 2016
Available online 26 July 2016

Keywords:
Mass conservative
Semi-Lagrangian scheme
HWENO reconstruction
Vlasov–Poisson system
Landau damping
Two-stream instability

ABSTRACT

In this paper, we propose a high order conservative semi-Lagrangian (SL) finite difference Hermite weighted essentially non-oscillatory (HWENO) method for the Vlasov equation based on dimensional splitting. HWENO was first proposed for solving nonlinear hyperbolic problems by evolving both function values and its first derivative values (Qiu and Shu (2004) [23]). The major advantage of HWENO, compared with the original WENO, lies in its compactness in reconstruction stencils.

There are several new ingredients in this paper. Firstly we propose a *mass-conservative* SL HWENO scheme for a 1-D equation by working with a flux-difference form, following the work of Qiu and Christlieb (2010) [25]. Secondly, we propose a proper splitting for equations of partial derivatives in HWENO framework to ensure local mass conservation. The proposed fifth order SL HWENO scheme with dimensional splitting has been tested to work well in capturing filamentation structures without oscillations when the time step size is within the Eulerian CFL constraint. However, when the time stepping size becomes larger, numerical oscillations are observed for the 'mass conservative' dimensional splitting HWENO scheme, as there are extra source terms in equations of partial derivatives. In this case, we introduce WENO limiters to control oscillations. Classical numerical examples on linear passive transport problems, as well as the nonlinear Vlasov–Poisson system, have been tested to demonstrate the performance of the proposed scheme.

1. Introduction

This paper focuses on a mass conservative semi-Lagrangian scheme with high order Hermite weighted essentially non-oscillatory (HWENO) reconstruction for the Vlasov–Poisson (VP) simulations based on dimensional splitting. The VP system, arising from collisionless plasma applications, reads as follows,

$$\frac{\partial f}{\partial t} + \mathbf{v} \cdot \nabla_{\mathbf{x}} f + \mathbf{E}(t, \mathbf{x}) \cdot \nabla_{\mathbf{v}} f = 0, \tag{1.1}$$

☆ Research was partially supported by NSFC Grants 91230110, 11328104, 11571290, 91530107 and NSF DMS-1217008 and DMS-1522777.
* Corresponding author.
E-mail addresses: xfcai89@126.com (X. Cai), jxqiu@xmu.edu.cn (J. Qiu), jingqiu@math.uh.edu (J.-M. Qiu).

http://dx.doi.org/10.1016/j.jcp.2016.07.021
0021-9991/

and

$$\mathbf{E}(t,\mathbf{x}) = -\nabla_{\mathbf{x}}\phi(t,\mathbf{x}), \quad -\Delta_{\mathbf{x}}\phi(t,\mathbf{x}) = \rho(t,\mathbf{x}), \tag{1.2}$$

where $\mathbf{x}$ and $\mathbf{v}$ are coordinates in phase space $(\mathbf{x},\mathbf{v}) \in \mathbb{R}^3 \times \mathbb{R}^3$, $\mathbf{E}$ is the electric field, ϕ is the self-consistent electrostatic potential and $f(t,\mathbf{x},\mathbf{v})$ is probability distribution function which describes the probability of finding a particle with velocity $\mathbf{v}$ at position $\mathbf{x}$ at time t. The probability distribution function couples to the long range fields via the charge density, $\rho(t,\mathbf{x}) = \int_{\mathbb{R}^3} f(t,\mathbf{x},\mathbf{v})d\mathbf{v} - 1$, where we take the limit of uniformly distributed infinitely massive ions in the background. Equations (1.1) and (1.2) have been nondimensionalized so that all physical constants are one.

Popular methods in fusion simulations include Lagrangian, semi-Lagrangian and Eulerian methods. Popular Lagrangian methods include the particle-in-cell (PIC) [2,15,18], Lagrangian particle methods [3,12]; Eulerian methods include weighted essentially non-oscillatory (WENO) coupled with Fourier collocation [37], continuous finite element methods [36,35], Runge–Kutta discontinuous Galerkin (DG) methods [1,11,17,8]. Each method has its own advantages and limitations. For example, Lagrangian methods are well known for their reasonably low computational cost for high dimensional problems. However, they suffer from statistical noise due to the initial sampling of macro-particles. Eulerian methods offer a good alternative to overcome this lack of precision, but they suffer from 'the curse of dimensionality' and the CFL time step restriction. Compared with the Eulerian approach, the SL method is free of the CFL time step restriction, because information is being propagated along characteristics.

A SL scheme for the VP simulation based on dimensional splitting was originally introduced by Cheng and Knorr [7]. Following this framework, there are various SL schemes with different solution spaces and reconstruction techniques. For example, a SL scheme with cubic spline interpolation was proposed [31]; a positivity preserving and flux conservative finite volume SL scheme with ENO reconstruction for the VP system and for the guiding center Vlasov model were proposed in [14,10] respectively. In [25], authors proposed a conservative finite difference SL WENO scheme, which was generalized to the variable coefficient case [26] and being applied to the VP simulation [27]. Recently in [33], a maximum principle preserving flux limiter is applied to the SL scheme to enforce positivity. In the finite element DG framework, there are SL DG schemes with positivity preserving limiters [28,29]. A hybrid SL finite element-finite difference method was proposed in [16]. Very closely related to the current work, there are SL methods with Hermite interpolation, in which functions' derivatives play an important role in building up high order schemes [22,13,5,4,34].

HWENO scheme was firstly introduced in [23] and further developed in [38,21] for hyperbolic conservation laws. Besides the original equation, one also evolves equations of derivatives in the WENO fashion. Hence their reconstruction stencils are more compact than the original WENO scheme [19], given the same order of approximation. In this paper, we couple the semi-Lagrangian framework with the HWENO method. There are several new ingredients, compared with existing ones in the literature. Firstly, we propose a SL HWENO scheme in a flux difference conservative form to ensure mass conservation for 1-D transport problems. Then the WENO procedure is applied to the fluxes for a robust capture of solutions with sharp gradients. Secondly, we apply a special splitting [22] to preserve the mass conservation for 2-D problems. On the other hand, such splitting introduces source terms (besides the regular transport terms) in the system. Due to a linear treatment of these source terms, oscillations are numerically observed when the time step size is larger than the Eulerian CFL constraint. To resolve such issues, we apply WENO limiters [24] wherever oscillations are detected.

The paper is organized as follows. In Section 2, we introduce a conservative SL HWENO method for 1-D transport problems. In Section 3, we introduce the scheme for the VP system by a special form of splitting that conserves the total mass. Wherever it is necessary, WENO limiters are applied to suppress oscillations. In Section 4, we present our numerical results for basic linear test problems, such as linear advection and rigid body rotation, and for the nonlinear VP simulations. Concluding remarks are given in Section 5.

2. Conservative SL HWENO method for 1-D transport problem

In this section, we introduce the SL Hermite interpolation in a flux-difference form for 1-D transport problems. Then we incorporate the HWENO mechanism into the flux function reconstruction procedure to realize a non-oscillatory capturing of solutions with sharp gradients.

2.1. The SL Hermite interpolation in a flux-difference form for 1-D transport problem

In this section, we consider a 1-D transport problem

$$f_t + vf_x = 0, \quad f(x,t=0) = f_0(x), \quad \text{on} \quad [a,b], \tag{2.1}$$

where v is a constant. For the Hermite method, we also consider the evolution equation for the solution's derivative $g \doteq f_x$. For the linear transport problem (2.1), g satisfies the same linear transport equation

$$g_t + vg_x = 0.$$

We discretize the domain $[a,b]$ as

$$a = x_{\frac{1}{2}} < x_{\frac{3}{2}} < \cdots < x_{N+\frac{1}{2}} = b,$$

with the uniform grid points $x_i = a + (i - \frac{1}{2})\Delta x$ and the cell size $\Delta x = x_{i+\frac{1}{2}} - x_{i-\frac{1}{2}}$. We let $I_i = [x_{i-\frac{1}{2}}, x_{i+\frac{1}{2}}]$ and $I_{i+\frac{1}{2}} = [x_i, x_{i+1}]$. In the HWENO approach, the numerical solutions associated with each grid point are point values f_i^n and derivatives g_i^n. Here the subscript i means the solution at the grid point x_i and the superscript n means the solution at time level t^n. To design a SL HWENO scheme, we update $\{f_i^{n+1}, g_i^{n+1}\}_{i=1}^N$ from the corresponding solutions at time t^n.

For the linear problem (2.1) with constant characteristic speed, the solutions f_i^{n+1} and g_i^{n+1} can be obtained by shifting the information at t^n in the SL framework. We define the amount of shift scaled by the mesh size as $xshift = v\Delta t/\Delta x$. There are three cases of $xshift$: shift to the right by some amount less than half a cell ($xshift \in [0, \frac{1}{2}]$), shift to the left by some amount less than half a cell ($xshift \in [-\frac{1}{2}, 0]$) and shift a distance greater than half a cell ($|xshift| > \frac{1}{2}$).

To illustrate the idea, we only consider Hermite interpolations for $xshift \in [0, \frac{1}{2}]$, while the one for $xshift \in [-\frac{1}{2}, 0]$ is mirror symmetric with respect to x_i of the previous interpolations. In the case when $|xshift| > \frac{1}{2}$, whole grid shifting is carried out and followed by a final update based on the procedure for $xshift \in [-\frac{1}{2}, \frac{1}{2}]$. In the following, we present the Hermite interpolation with cubic polynomials. Higher order schemes will be discussed later.

1. The underlying function at t^n can be approximated by a Hermite-type reconstruction, based on the stencil $\{f_{i-1}^n, f_i^n, g_{i-1}^n, g_i^n\}$,
$$\widetilde{f}_{i-\frac{1}{2}}^n(\xi) = f_i^n - g_i^n\Delta x\xi + \left(2g_i^n\Delta x - 3f_i^n + 3f_{i-1}^n + g_{i-1}^n\Delta x\right)\xi^2 + \left(2f_i^n - g_i^n\Delta x - 2f_{i-1}^n - g_{i-1}^n\Delta x\right)\xi^3,$$
where $\xi(x) = \frac{x - x_i}{x_{i-1} - x_i} \in [0, 1], x \in I_{i-\frac{1}{2}}$.
2. f_i^{n+1} and g_i^{n+1} can be obtained by tracing the characteristic back to time $t = t^n$ and evaluating the interpolant $\widetilde{f}_{i-\frac{1}{2}}^n(\xi)$ at the foot of characteristics $x^\star = x_i - v\Delta t$,
$$\begin{aligned} f_i^{n+1} &= f_i^n - \xi_0((3f_i^n\xi_0 - 2f_i^n\xi_0^2) - (3f_{i-1}^n\xi_0 - 2f_{i-1}^n\xi_0^2)) \\ &\quad - g_i^n\Delta x\xi_0 + (2g_i^n\Delta x + g_{i-1}^n\Delta x)\xi_0^2 + (-g_i^n\Delta x - g_{i-1}^n\Delta x)\xi_0^3 \end{aligned} \tag{2.2}$$
$$g_i^{n+1} = g_i^n + \left(-4g_i^n + \frac{6f_i^n - 6f_{i-1}^n}{\Delta x} - 2g_{i-1}^n\right)\xi_0 + \left(-\frac{6f_i^n - f_{i-1}^n}{\Delta x} + 3g_i^n + 3g_{i-1}^n\right)\xi_0^2, \tag{2.3}$$
where $\xi_0 = \frac{x^\star - x_i}{x_{i-1} - x_i}$.

For the above linear scheme (2.2) and (2.3), we have the following mass conservation result.

Proposition 1. *If $\sum_{i=1}^N g_i^n \equiv 0$ and with periodic boundary condition, then the scheme (2.2) and (2.3) conserve the total mass, i.e., $\sum_{i=1}^N f_i^{n+1} \equiv \sum_{i=1}^N f_i^n$ and $\sum_{i=1}^N g_i^{n+1} \equiv 0$.*

Proof.
$$\begin{aligned} \sum_{i=1}^N f_i^{n+1} &= \sum_{i=1}^N [f_i^n - \xi_0((3f_i^n\xi_0 - 2f_i^n\xi_0^2) - (3f_{i-1}^n\xi_0 - 2f_{i-1}^n\xi_0^2)) \\ &\quad - g_i^n\Delta x\xi_0 + (2g_i^n\Delta x + g_{i-1}^n\Delta x)\xi_0^2 + (-g_i^n\Delta x - g_{i-1}^n\Delta x)\xi_0^3] \\ &= \sum_{i=1}^N f_i^n - \xi_0((3f_N^n\xi_0 - 2f_N^n\xi_0^2) - (3f_0^n\xi_0 - 2f_0^n\xi_0^2)) + \sum_{i=1}^N g_{i-1}^n\Delta x\xi_0^2 - \sum_{i=1}^N g_{i-1}^n\Delta x\xi_0^3 \\ &= \sum_{i=1}^N f_i^n \text{ (periodic boundary condition)}, \end{aligned}$$
$$\begin{aligned} \sum_{i=1}^N g_i^{n+1} &= \sum_{i=1}^N \left[g_i^n + \left(-4g_i^n + \frac{6f_i^n - 6f_{i-1}^n}{\Delta x} - 2g_{i-1}^n\right)\xi_0 + \left(-\frac{6f_i^n - f_{i-1}^n}{\Delta x} + 3g_i^n + 3g_{i-1}^n\right)\xi_0^2\right] \\ &= \sum_{i=1}^N g_i^n + \frac{6f_N^n - 6f_0^n}{\Delta x}\xi_0 - \frac{6f_N^n - f_0^n}{\Delta x}\xi_0^2 + 2\sum_{i=1}^N g_{i-1}^n\Delta x\xi_0^2 - 3\sum_{i=1}^N g_{i-1}^n\Delta x\xi_0^3 \\ &= \sum_{i=1}^N g_i^n \text{ (periodic boundary condition)}. \end{aligned}$$
Hence the proposition is proved. □

In order to guarantee $\sum_{i=1}^{N} g_i^0 \equiv 0$ in the assumption of the proposition, we introduce a sliding average function $h(x)$ in [30] which satisfies

$$f(x) = \frac{1}{\Delta x} \int_{x-\frac{\Delta x}{2}}^{x+\frac{\Delta x}{2}} h(\xi) d\xi,$$

then

$$g(x) = f(x)_x = \frac{1}{\Delta x}\left(h\left(x+\frac{\Delta x}{2}\right) - h\left(x-\frac{\Delta x}{2}\right)\right).$$

Thus $\sum_{i=1}^{N} g_i^0 = \sum_{i=1}^{N} (h_{i+\frac{1}{2}}^0 - h_{i-\frac{1}{2}}^0) \equiv 0$ where $h_{i\pm\frac{1}{2}}^0 \approx h(x \pm \frac{\Delta x}{2})$ can be obtained by reconstruction from $\{f_j^0\}_j$. In this paper, we adopt the fifth order upwind-biased WENO reconstruction for obtaining initial conditions of h. In fact, if $v > 0$, we adopt $\{f_{i-2}^0, f_{i-1}^0, f_i^0, f_{i+1}^0, f_{i+2}^0\}$ to reconstruct $h_{i+\frac{1}{2}}^0$; if $v \le 0$, $h_{i+\frac{1}{2}}^0$ is reconstructed by $\{f_{i-1}^0, f_i^0, f_{i+1}^0, f_{i+2}^0, f_{i+3}^0\}$.

In the following, we will adopt a matrix notation for presentation of the Hermite interpolation. The matrix A will denote the interpolation matrix. We use $A(i, j)$ to denote the element at the ith row and jth column, $A(i, :)$ to denote the ith row of A, and $A(:, j)$ to denote the jth column of A.

We rewrite the scheme (2.2) and (2.3) into a flux difference form, in order to ensure local mass conservation, especially when the nonlinear HWENO mechanism is applied. In order to do so, we propose to update $\{f_i^n, h_{i+\frac{1}{2}}^n\}_i$ instead of $\{f_i^n, g_i^n\}_i$, observing that g_i^n can be recovered from $\{h_{i+\frac{1}{2}}^n\}_i$ by $g_i^n = \left(h_{i+\frac{1}{2}}^n - h_{i-\frac{1}{2}}^n\right)/\Delta x$. Specifically, (2.2) can be rewritten in the following flux difference form using the new $\{h_{i+\frac{1}{2}}^n\}_i$,

$$\begin{aligned}
f_i^{n+1} &= f_i^n - \xi_0(f_i^n(3\xi_0 - 2\xi_0^2) - f_{i-1}^n(3\xi_0 - 2\xi_0^2)) + g_i^n \Delta x(-\xi_0 + 2\xi_0^2 - \xi_0^3) + g_{i-1}^n \Delta x(\xi_0^2 - \xi_0^3) \\
&= f_i^n - \xi_0(f_i^n(3\xi_0 - 2\xi_0^2) - f_{i-1}^n(3\xi_0 - 2\xi_0^2)) \\
&\quad - \left(h_{i+\frac{1}{2}}^n - h_{i-\frac{1}{2}}^n\right)\xi_0(1 - 2\xi_0 + \xi_0^2) - \left(h_{i-\frac{1}{2}}^n - h_{i-\frac{3}{2}}^n\right)\xi_0(-\xi_0 + \xi_0^2) \\
&= f_i^n - \xi_0\left\{\left[f_i^n(3\xi_0 - \xi_0^2) + h_{i+\frac{1}{2}}^n(1 - 2\xi_0 + \xi_0^2) + h_{i-\frac{1}{2}}^n(-\xi_0 - \xi_0^2)\right]\right. \\
&\quad \left. - \left[f_{i-1}^n(3\xi_0 - \xi_0^2) + h_{i-\frac{1}{2}}^n(1 - 2\xi_0 + \xi_0^2) + h_{i-\frac{3}{2}}^n(-\xi_0 - \xi_0^2)\right]\right\} \\
&= f_i - \xi_0(\widehat{f}_{i+\frac{1}{2}}^n(\xi_0) - \widehat{f}_{i-\frac{1}{2}}^n(\xi_0)),
\end{aligned}$$

where

$$\widehat{f}_{i-\frac{1}{2}}^n(\xi_0) = (f_{i-1}^n, h_{i-\frac{1}{2}}^n, h_{i-\frac{3}{2}}^n) \cdot C_3^L \cdot (1, \xi_0, \xi_0^2)'$$

with

$$C_3^L = \begin{pmatrix} 0 & 3 & -2 \\ 1 & -2 & 1 \\ 0 & -1 & 1 \end{pmatrix}.$$

We update g_i^{n+1} by

$$g_i^{n+1} = \frac{h_{i+\frac{1}{2}}^{n+1} - h_{i-\frac{1}{2}}^{n+1}}{\Delta x}, \tag{2.4}$$

where

$$h_{i-\frac{1}{2}}^{n+1} = (f_{i-1}^n, h_{i-\frac{1}{2}}^n, h_{i-\frac{3}{2}}^n) \cdot D_3^L \cdot (1, \xi_0, \xi_0^2)' \tag{2.5}$$

with

$$D_3^L = \begin{pmatrix} 0 & 6 & -6 \\ 1 & -4 & 3 \\ 0 & -2 & 3 \end{pmatrix}.$$

Remark 1. The flux-difference form for the SL finite difference scheme was originally proposed in [25]. There are two main advantages to work with the flux difference form:

1. The flux difference form can ensure local mass conservation.
2. We can design a nonlinear HWENO mechanism for the flux reconstructions, see discussions in the next subsection.

In order to work with the flux difference form, it is crucial to work with the $\{h^n_{i+\frac{1}{2}}\}_i$ instead of the original derivative function $g = f_x$. Notice that one important assumption in Proposition 1 is that $\sum g^n_i = 0$. If we let g^n_i be the exact value of function derivatives, $\sum g^n_i$ is small ($\approx \Delta x^r$ with r being the order of approximation) when the function is smooth and $\sum g^n_i$ can be far away from zero if the function has sharp gradients. In general, $\sum g^n_i = 0$ is not necessarily true, unless one works with the flux form.

Remark 2. The case presented here is for the third order scheme. We observe that $D^L_3(:,k) = kC^L_3(:,k)$, $k = 1,2,3$. Similar procedure can be used to obtained higher order scheme, e.g. the fifth order case with HWENO is presented in the next subsection.

2.2. HWENO reconstruction for flux functions

In general, high order fixed stencil reconstruction of numerical fluxes performs well when the solution is smooth. However, around discontinuities, oscillations will be introduced. In this subsection, a nonlinear SL HWENO procedure is introduced for reconstructing the flux $\widehat{f}^n_{i-\frac{1}{2}}(\xi)$. By adaptively assigning nonlinear weights to neighboring candidate stencils, the nonlinear HWENO reconstruction preserves high order accuracy of the linear scheme around smooth regions of the solution, while producing a sharp and essentially non-oscillatory capture of discontinuities.

We adopt the idea of the HWENO reconstruction [23,21] into the proposed conservative SL framework. We present a fifth order HWENO reconstruction as an example. Similar procedure can be generalized to higher order case.

Our discussion will be focused on the case of $xshift \in [-\frac{1}{2}, \frac{1}{2}]$. As before, the case of $|xshift| > \frac{1}{2}$ will be handled with a whole grid shift followed by the case of $xshift \in [-\frac{1}{2}, \frac{1}{2}]$ to account for the fractional remainder.

When $xshift \in [0, \frac{1}{2}]$, the fifth order conservative SL method based on the reconstruction stencil $\{f^n_{i-2}, f^n_{i-1}, f^n_i, f^n_{i+1}, g^n_{i-2}, g^n_{i+1}\}$ is the following,

$$\begin{aligned}
f^{n+1}_i = f^n_i &+ \left(-\frac{8}{27}f^n_{i-2} + f^n_{i-1} - \frac{19}{27}f^n_{i+1} + \frac{2}{9}g^n_{i+1}\Delta x - \frac{1}{9}g^n_{i-2}\Delta x\right)\xi_0 \\
&+ \left(-\frac{1}{18}g^n_{i-2}\Delta x - \frac{2}{9}g^n_{i+1}\Delta x - \frac{7}{4}f^n_i - \frac{19}{108}f^n_{i-2} + f^n_{i-1} + \frac{25}{27}f^n_{i+1}\right)\xi_0^2 \\
&+ \left(\frac{1}{6}g^n_{i-2}\Delta x - \frac{1}{6}g^n_{i+1}\Delta x + \frac{1}{4}f^n_i + \frac{5}{12}f^n_{i-2} - \frac{3}{4}f^n_{i-1} + \frac{1}{12}f^n_{i+1}\right)\xi_0^3 \\
&+ \left(\frac{1}{18}g^n_{i-2}\Delta x + \frac{2}{9}g^n_{i+1}\Delta x + \frac{3}{4}f^n_i + \frac{19}{108}f^n_{i-2} - \frac{1}{2}f^n_{i-1} - \frac{23}{54}f^n_{i+1}\right)\xi_0^4 \\
&+ \left(-\frac{1}{18}g^n_{i-2}\Delta x - \frac{1}{18}g^n_{i+1}\Delta x - \frac{1}{4}f^n_i - \frac{13}{108}f^n_{i-2} + \frac{1}{4}f^n_{i-1} + \frac{13}{108}f^n_{i+1}\right)\xi_0^5.
\end{aligned}$$

Using the flux difference form for g function, $g^n_i = \frac{h^n_{i+\frac{1}{2}} - h^n_{i-\frac{1}{2}}}{\Delta x}$, then

$$f^{n+1}_i = f^n_i - \xi_0((f^n_{i-2}, f^n_{i-1}, f_i, f^n_{i+1}, h^n_{i-\frac{5}{2}}, h^n_{i-\frac{3}{2}}, h^n_{i+\frac{1}{2}}, h^n_{i+\frac{3}{2}}) \cdot B^L_5 \cdot (1, \xi_0, \xi_0^2, \xi_0^3, \xi_0^4)')$$

where

$$B^L_5 = \begin{pmatrix}
\frac{8}{27} & \frac{19}{108} & -\frac{5}{12} & -\frac{19}{108} & \frac{13}{108} \\
-1 & -1 & \frac{3}{4} & \frac{1}{2} & -\frac{1}{4} \\
0 & \frac{7}{4} & -\frac{1}{4} & -\frac{3}{4} & \frac{1}{4} \\
\frac{19}{27} & -\frac{25}{27} & -\frac{1}{12} & \frac{23}{54} & -\frac{13}{108} \\
-\frac{1}{9} & -\frac{1}{18} & \frac{1}{6} & \frac{1}{18} & -\frac{1}{18} \\
\frac{1}{9} & \frac{1}{18} & -\frac{1}{6} & -\frac{1}{18} & \frac{1}{18} \\
\frac{2}{9} & -\frac{2}{9} & -\frac{1}{6} & \frac{2}{9} & -\frac{1}{18} \\
-\frac{2}{9} & \frac{2}{9} & \frac{1}{6} & -\frac{2}{9} & \frac{1}{18}
\end{pmatrix}.$$

Then f_i^{n+1} can be written in the flux difference form,

$$f_i^{n+1} = f_i^n - \xi_0((f_{i-1}^n, f_i^n, f_{i+1}^n, h_{i-\frac{3}{2}}^n, h_{i+\frac{3}{2}}^n) \cdot C_5^L - (f_{i-2}^n, f_{i-1}^n, f_i^n, h_{i-\frac{5}{2}}^n, h_{i+\frac{1}{2}}^n) \cdot C_5^L) \cdot (1, \xi_0, \xi_0^2, \xi_0^3, \xi_0^4)' \tag{2.6}$$

where

$$C_5^L = \begin{pmatrix} -\frac{8}{27} & -\frac{19}{108} & \frac{5}{12} & \frac{19}{108} & -\frac{13}{108} \\ \frac{19}{27} & \frac{89}{108} & -\frac{1}{3} & -\frac{35}{108} & \frac{7}{54} \\ \frac{19}{27} & -\frac{25}{27} & -\frac{1}{12} & \frac{23}{54} & -\frac{13}{108} \\ \frac{1}{9} & \frac{1}{18} & -\frac{1}{6} & -\frac{1}{18} & \frac{1}{18} \\ -\frac{2}{9} & \frac{2}{9} & \frac{1}{6} & -\frac{2}{9} & \frac{1}{18} \end{pmatrix}.$$

And we have the flux difference form the derivative g_i^{n+1} in t^{n+1},

$$g_i^{n+1} = \frac{h_{i+\frac{1}{2}}^{n+1} - h_{i-\frac{1}{2}}^{n+1}}{\Delta x}$$

where

$$h_{i-\frac{1}{2}}^{n+1} = (f_{i-2}^n, f_{i-1}^n, f_i^n, h_{i-\frac{5}{2}}^n, h_{i+\frac{1}{2}}^n) \cdot D_5^L \cdot (1, \xi_0, \xi_0^2, \xi_0^3, \xi_0^4)' \tag{2.7}$$

where D_5^L satisfies $D_5^L(:,k) = kC_5^L(:,k)$, $k = 1, \cdots, 5$.

When $xshift \in [-\frac{1}{2}, 0]$, we update $\{f_i^{n+1}, h_{i+\frac{1}{2}}^{n+1}\}_i$ by the following formulas,

$$f_i^{n+1} = f_i^n + \xi_0(\widehat{f}_{i+\frac{1}{2}}^n(\xi_0) - \widehat{f}_{i-\frac{1}{2}}^n(\xi_0)), \tag{2.8}$$

where the flux function

$$\widehat{f}_{i-\frac{1}{2}}^n(\xi) = (f_{i-1}^n, f_i^n, f_{i+1}^n, h_{i-\frac{3}{2}}, h_{i+\frac{3}{2}}) \cdot C_5^R \cdot (1, \xi_0, \xi_0^2, \xi_0^3, \xi_0^4)', \tag{2.9}$$

where

$$C_5^R = \begin{pmatrix} \frac{19}{27} & -\frac{25}{27} & -\frac{1}{12} & \frac{23}{54} & -\frac{13}{108} \\ \frac{19}{27} & \frac{89}{108} & -\frac{1}{3} & -\frac{35}{108} & \frac{7}{54} \\ -\frac{8}{27} & -\frac{19}{108} & \frac{5}{12} & \frac{19}{108} & -\frac{13}{108} \\ -\frac{2}{9} & \frac{2}{9} & \frac{1}{6} & -\frac{2}{9} & \frac{1}{18} \\ \frac{1}{9} & \frac{1}{18} & -\frac{1}{6} & -\frac{1}{18} & \frac{1}{18} \end{pmatrix}, \tag{2.10}$$

and

$$h_{i-\frac{1}{2}}^{n+1} = (f_{i-1}^n, f_i^n, f_{i+1}^n, h_{i-\frac{3}{2}}^n, h_{i+\frac{3}{2}}^n) \cdot D_5^R \cdot (1, \xi_0, \xi_0^2, \xi_0^3, \xi_0^4)', \tag{2.11}$$

where D_5^R satisfies $D_5^R(:,k) = kC_5^R(:,k)$, $k = 1, \cdots, 5$.

In the following, we illustrate the corresponding HWENO reconstruction of flux functions. We only discuss the HWENO reconstruction for the flux $\widehat{f}_{i-\frac{1}{2}}^n$ and $h_{i-\frac{1}{2}}^{n+1}$ when $xshift \in [0, \frac{1}{2}]$. When $xshift \in [-\frac{1}{2}, 0]$, the flux $\widehat{f}_{i-\frac{1}{2}}^n$ and $h_{i-\frac{1}{2}}^{n+1}$ could be reconstructed symmetrically with respect to x_i. From equations (2.6) and (2.7), the stencil $\{f_{i-2}^n, f_{i-1}^n, f_i^n, h_{i-\frac{5}{2}}^n, h_{i+\frac{1}{2}}^n\}$ is used to construct the flux $\widehat{f}_{i-\frac{1}{2}}^n(\xi)$ and $h_{i-\frac{1}{2}}^{n+1}$. It is composed of the information from three potential stencils

$$S_1 = \{h_{i-\frac{5}{2}}^n, f_{i-2}^n, f_{i-1}^n\},\ S_2 = \{f_{i-2}^n, f_{i-1}^n, f_i^n\},\ S_3 = \{f_{i-1}^n, f_i^n, h_{i+\frac{1}{2}}^n\}. \tag{2.12}$$

Intuitively, in regions where the function is smooth, we want to use information from S_1, S_2 and S_3 in an optimal way, to obtain a fifth order approximation. On the other hand, around a big jump, we only want to use the information from the relatively smooth stencil. Following [25], we only use the HWENO mechanism in adaptively reconstructing the coefficients in front of the constant 1 in the equation for $\widehat{f}_{i-\frac{1}{2}}^n$ and $h_{i-\frac{1}{2}}^{n+1}$, while leaving coefficients for $\xi_0, \xi_0^2, \xi_0^3, \xi_0^4$ unchanged. We can observe that the first column of matrix C_5^L is the same as that of D_5^L. Thus we only consider the HWENO procedure for constructing $\widehat{f}_{i-\frac{1}{2}}^n$,

1. Compute the linear weights, γ_1, γ_2 and γ_3, such that

$$
\begin{aligned}
&(f^n_{i-2}, f^n_{i-1}, f^n_i, h^n_{i-\frac{5}{2}}, h^n_{i+\frac{1}{2}}) \cdot C^L_5(:,1) \\
&= \gamma_1 (f^n_{i-2}, f^n_{i-1}, h^n_{i-\frac{5}{2}}) \cdot (-2,2,1)' + \gamma_2 (f^n_{i-2}, f^n_{i-1}, f^n_i) \cdot (-\frac{1}{6}, \frac{5}{6}, \frac{1}{3})' \\
&+ \gamma_3 (f^n_{i-1}, f^n_i, h^n_{i+\frac{1}{2}}) \cdot (\frac{1}{4}, \frac{5}{4}, -\frac{1}{2})',
\end{aligned}
$$

where $(f^n_{i-2}, f^n_{i-1}, h^n_{i-\frac{5}{2}}) \cdot (-2,2,1)'$, $(f^n_{i-2}, f^n_{i-1}, f^n_i) \cdot (-\frac{1}{6}, \frac{5}{6}, \frac{1}{3})'$ and $(f^n_{i-1}, f^n_i, h^n_{i+\frac{1}{2}}) \cdot (\frac{1}{4}, \frac{5}{4}, -\frac{1}{2})'$ are third order reconstructions of fluxes from three stencils S_1, S_2 and S_3, respectively. From equation (2.6), $\gamma_1 = \frac{1}{9}$, $\gamma_2 = \frac{4}{9}$ and $\gamma_3 = \frac{4}{9}$.

2. We compute the smoothness indicator, denoted by β_j, for each stencil S_j, which measures how smooth the function $p_j(x)$ is in the target cell I_i. The smaller this smoothness indicator β_j, the smoother the function $p_j(x)$ is in the target cell. We use the same recipe for the smoothness indicator as in [19],

$$
\beta_j = \sum_{l=1}^{2} \int_{I_i} \Delta x^{2l-1} \left(\frac{\partial}{\partial x^l} p_j(x) \right)^2 dx.
$$

In the actual numerical implementation the smoothness indicators β_j are written out explicitly as quadratic forms of the points $\{f^n_i, h^n_{i+\frac{1}{2}}\}_i$ in the stencil,

$$
\begin{aligned}
\beta_1 &= \frac{13}{3} \left(-\frac{9}{4} f^n_{i-2} + \frac{3}{2} h^n_{i-\frac{5}{2}} + \frac{3}{4} f^n_{i-1} \right)^2 + \left(\frac{31}{4} f^n_{i-2} - \frac{9}{2} h^n_{i-\frac{5}{2}} - \frac{13}{4} f^n_{i-1} \right)^2, \\
\beta_2 &= \frac{13}{12} \left(-f^n_{i-2} + 2 f^n_{i-1} - f^n_i \right)^2 + \left(-\frac{3}{2} f^n_i + 2 f^n_{i-1} - \frac{1}{2} f^n_{i-2} \right)^2, \\
\beta_3 &= \frac{13}{3} \left(-\frac{9}{4} f^n_i + \frac{3}{4} f^n_{i-1} + \frac{3}{2} h^n_{i+\frac{1}{2}} \right)^2 + \left(\frac{5}{4} f^n_i + \frac{1}{4} f^n_{i-1} - \frac{3}{2} h^n_{i+\frac{1}{2}} \right)^2.
\end{aligned}
$$

3. We compute the nonlinear weights based on the smoothness indicators.

$$
\omega_j = \frac{\overline{\omega}_j}{\sum_{k=1}^{3} \overline{\omega}_k}, \ j = 1,2,3, \quad \overline{\omega}_k = \frac{\gamma_k}{(\epsilon + \beta_k)^2}
$$

where ϵ is a small number to prevent the denominator from becoming zero. In our numerical tests we take ϵ to be 10^{-6}.

4. Compute numerical fluxes constructed in HWENO fashion. Define the matrix $\widetilde{C}^L_5$ and $\widetilde{D}^L_5$ as,

$$
\begin{aligned}
&\widetilde{D}^L_5(:,1) = \widetilde{C}^L_5(:,1) = \omega_1 \cdot (-2,2,0,1,0) + \omega_2 \cdot (-\frac{1}{6}, \frac{5}{6}, \frac{1}{3}, 0, 0) + \omega_3 \cdot (0, \frac{1}{4}, \frac{5}{4}, 0, -\frac{1}{2}) \\
&\widetilde{C}^L_5(:,k) = C^L_5(:,k), \ \widetilde{D}^L_5(:,2) = k C^L_5(:,k), \ k = 2, \cdots, 5.
\end{aligned}
$$

The updated numerical flux is computed using $\widetilde{C}^L_5$ and $\widetilde{D}^L_5$, i.e.,

$$
\widehat{f}^n_{i-\frac{1}{2}}(\xi_0) = (f^n_{i-2}, f^n_{i-1}, f^n_i, h^n_{i-\frac{5}{2}}, h^n_{i+\frac{1}{2}}) \cdot \widetilde{C}^L_5 \cdot (1, \xi_0, \xi_0^2, \xi_0^3, \xi_0^4)', \tag{2.13}
$$

$$
h^{n+1}_{i-\frac{1}{2}} = (f^n_{i-2}, f^n_{i-1}, f^n_i, h^n_{i-\frac{5}{2}}, h^n_{i+\frac{1}{2}}) \cdot \widetilde{D}^L_5 \cdot (1, \xi_0, \xi_0^2, \xi_0^3, \xi_0^4)'. \tag{2.14}
$$

3. Strang splitting SL HWENO scheme for the VP system

In this section, we extend the SL HWENO scheme in the previous section for solving the 1-D VP system.

Denoting by $f(t,x,v) \geq 0$ the distribution function of electrons in phase space and by $E(t,x)$ the self-consistent electric field, the dimensionless VP systems reads as

$$
\frac{\partial f}{\partial t} + v \frac{\partial f}{\partial x} + E(t,x) \frac{\partial f}{\partial v} = 0, \tag{3.1}
$$

$$
\frac{dE}{dx}(t,x) = \rho(t,x) = \int_{-\infty}^{+\infty} f(t,x,v) dv - 1, \tag{3.2}
$$

on the domain $[a,b]\times[-L,L]$ with periodic boundary condition for the spatial domain and zero boundary condition for the velocity domain.

For the Hermite method, we advect not only the distribution function f but also its derivatives in x and in v directions. We have the following equations for f_x and f_v,

$$\begin{cases} \frac{\partial f_x}{\partial t}+v\frac{\partial f_x}{\partial x}+\frac{\partial (E(t,x)f_v)}{\partial x}=0, \\ \frac{\partial f_v}{\partial t}+\frac{\partial (vf_x)}{\partial v}+E(t,x)\frac{\partial f_v}{\partial v}=0. \end{cases} \tag{3.3}$$

In this section, the SL HWENO scheme evolves this system based on the Strang splitting method [7]. The set of governing equations (3.1) and (3.3) in the Strang splitting method is replaced by

$$(SL_x)\begin{cases} \frac{\partial f}{\partial t}+v\frac{\partial f}{\partial x}=0 & (SL_x^0) \\ \frac{\partial f_x}{\partial t}+v\frac{\partial f_x}{\partial x}=0 & (SL_x^1) \\ \frac{\partial f_v}{\partial t}+\frac{\partial (vf_x)}{\partial v}=0 & (FD_x) \end{cases} \tag{3.4}$$

and

$$(SL_v)\begin{cases} \frac{\partial f}{\partial t}+E(t,x)\frac{\partial f}{\partial v}=0 & (SL_v^0) \\ \frac{\partial f_v}{\partial t}+E(t,x)\frac{\partial f_v}{\partial v}=0 & (SL_v^1) \\ \frac{\partial f_x}{\partial t}+\frac{\partial (E(t,x)f_v)}{\partial x}=0 & (FD_v) \end{cases}. \tag{3.5}$$

In the following, we present the proposed procedure of coupling 1-D SL HWENO solver for transport equation with dimensional splitting for the VP system. We discretize the computational domain $[a,b]\times[-L,L]$ as

$$a=x_{\frac12}<x_{\frac32}<\cdots<x_{N_x+\frac12}=b,\quad -L=v_{\frac12}<v_{\frac32}<\cdots<v_{N_v+\frac12}=L,$$

with uniformly distributed grid points $x_i=a+(i-\frac12)\Delta x$, $v_j=-L+(j-\frac12)\Delta v$, where grid spacing $\Delta x=x_{i+\frac12}-x_{i-\frac12}$, $\Delta v=v_{j+\frac12}-v_{j-\frac12}$. We let $I_i=[x_{i-\frac12},x_{i+\frac12}]$, $\forall i=1,\cdots,N_x$, $J_j=[v_{j-\frac12},v_{j+\frac12}]$, $\forall j=1,\cdots,N_v$ and $T_{ij}=[x_{i-\frac12},x_{i+\frac12}]\times[v_{j-\frac12},v_{j+\frac12}]$. We let f_{ij}^n, $(f_x)_{ij}^n$ and $(f_v)_{ij}^n$ denote the numerical approximation to the solution $f(x_i,v_j)$, $f_x(x_i,v_j)$, $f_v(x_i,v_j)$ at the time t^n respectively. Similar to the 1-D problem, we introduce $\{\Phi^n_{i-\frac12,j}\}_{ij}$ and $\{\Psi^n_{i,j-\frac12}\}_{ij}$ such that

$$(f_x)_{ij}^n=\frac{\Phi^n_{i+\frac12,j}-\Phi^n_{i-\frac12,j}}{\Delta x},\quad (f_v)_{ij}^n=\frac{\Psi^n_{i,j+\frac12}-\Psi^n_{i,j-\frac12}}{\Delta v}.$$

To evolve the VP system for a time step, we first solve the system (SL_x) for half a time step, then the system (SL_v) for a time step, and finally solve again the system (SL_x) for half a time step. Below, we focus our discussion on solving (SL_x). The scheme for (SL_v) would be similar.

Initialization: We use the high order WENO scheme in [19] to reconstruct $\{\Phi^0_{i+\frac12,j}\}$ and $\{\Psi^0_{i,j+\frac12}\}$ in x-direction and v-direction respectively as described for 1-D SL HWENO solver.

Update: We update $\{f_{ij}^n,\Phi^n_{i+\frac12,j}\}_{ij}$ by the 1-D SL HWENO scheme in Section 2. We update $\Psi^n_{i,j+\frac12}$ by the third equation in (3.4) via treating the derivative term as a source term. In particular, we apply the following a central difference scheme coupled with a trapezoid rule for (FD_x),

$$\begin{aligned}(f_v)_{ij}^{n+1}=(f_v)_{ij}^n-\frac{\Delta t}{2}\Bigg(&\frac{v_{i,j-2}(f_x)^n_{i,j-2}-8v_{i,j-1}(f_x)^n_{i,j-1}+8v_{i,j+1}(f_x)^n_{i,j+1}-v_{i,j+2}(f_x)^n_{i,j+2}}{24\Delta v}\\ &\frac{v_{i,j-2}(f_x)^{n+1}_{i,j-2}-8v_{i,j-1}(f_x)^{n+1}_{i,j-1}+8v_{i,j+1}(f_x)^{n+1}_{i,j+1}-v_{i,j+2}(f_x)^{n+1}_{i,j+2}}{24\Delta v}\Bigg),\end{aligned} \tag{3.6}$$

where

$$(f_x)_{ij}^*=\frac{\Phi^*_{i+\frac12,j}-\Phi^*_{i-\frac12,j}}{\Delta x},\ *=n,n+1,\quad (f_v)_{ij}^n=\frac{\Psi^n_{i,j+\frac12}-\Psi^n_{i,j-\frac12}}{\Delta v}. \tag{3.7}$$

Notice that $\{(f_x)_{ij}^{n+1}\}$ is available explicitly from the previous step of evolving SL_x^1. Equivalently, the scheme (3.6) can be rewritten for updating $\{\Psi^n_{i,j-\frac12}\}_{ij}$ with

$$\Psi^{n+1}_{i,j-\frac{1}{2}} = \Psi^{n}_{i,j-\frac{1}{2}} - \frac{\Delta t}{2}\left(\frac{-v_{i,j-2}(f_x)^n_{i,j-2} + 7v_{i,j-1}(f_x)^n_{i,j-1} + 7v_{i,j}(f_x)^n_{i,j} - v_{i,j+1}(f_x)^n_{i,j+1}}{24}\right.$$
$$\left. + \frac{-v_{i,j-2}(f_x)^{n+1}_{i,j-2} + 7v_{i,j-1}(f_x)^{n+1}_{i,j-1} + 7v_{ij}(f_x)^{n+1}_{ij} - v_{i,j+1}(f_x)^{n+1}_{i,j+1}}{24}\right). \tag{3.8}$$

From (3.8) and the fact that $(f_v)^{n+1}_{ij} = \frac{\Psi^{n+1}_{i,j+\frac{1}{2}} - \Psi^{n+1}_{i,j-\frac{1}{2}}}{\Delta v}$, we obtain (3.6), which provides a fourth order central difference for spatial discretization and a second order trapezoid rule for time integration. Because the k-th order on derivative values is enough to get a $(k+1)$-th order scheme, the scheme is fifth order in space. Since the Strang splitting introduces a second order error in time, the second order trapezoid rule will not affect the temporal accuracy of the scheme. Notice that there is no WENO mechanism in suppressing numerical oscillations involved in this step. In our numerical tests, we do observe oscillations, for which the WENO limiter is applied.

There is another equivalent form of governing equations for f, f_x and f_v [5,4],

$$\begin{cases} \frac{\partial f}{\partial t} + v\frac{\partial f}{\partial x} + E(t,x)\frac{\partial f}{\partial v} = 0, \\ \frac{\partial f_x}{\partial t} + v\frac{\partial f_x}{\partial x} + \frac{\partial E(t,x)}{\partial x} f_v + E(t,x)\frac{\partial f_x}{\partial v} = 0, \\ \frac{\partial f_v}{\partial t} + f_x + v\frac{\partial f_v}{\partial x} + E(t,x)\frac{\partial f_v}{\partial v} = 0. \end{cases} \tag{3.9}$$

Then in the context of operator splitting, the third equation in (3.4) will be

$$\frac{\partial f_v}{\partial t} + f_x + v\frac{\partial f_v}{\partial x} = 0. \tag{3.10}$$

We can design the SL scheme for the transport part $\frac{\partial f_v}{\partial t} + v\frac{\partial f_v}{\partial x} = 0$. However, due to the source term f_x, the scheme is not mass conservative for f_v. In other words, it leads to the difficulty for writing $(f_v)^n_{ij}$ in a flux difference form as $(f_v)^n_{ij} = \frac{\Psi^n_{i,j+\frac{1}{2}} - \Psi^n_{i,j-\frac{1}{2}}}{\Delta v}$. Only by working with the form (FD_x) in system (3.4), one can express f_v in a flux form. In this case, the term $\frac{\partial (v f_x)}{\partial v}$ is viewed as a source term, instead of a transport term. Note that when the term $\frac{\partial (v f_x)}{\partial v}$ is treated as a source term, there is time step constraint from the ODE stability (not the regular CFL condition in PDE). Further more, the spatial discretization in equation (3.6) or (3.8) does not involve any mechanism in suppressing oscillations. This explains the oscillations observed for large time step, hence the use of WENO limiters which is being discussed next.

This SL HWENO scheme may produce oscillations in large time stepping size when it simulates the VP system, mainly due to the treatment of source terms in (FD_x) and (FD_v) in system (3.4) and (3.5) respectively. We propose to apply the WENO limiter [23,24] before HWENO evolution as a pre-processing procedure which is similar to the procedure in [16]. We use the TVB limiter [9,23,24] with problem dependent TVB constants to identify troubled cells. For details of the procedure of the limiter, we refer to [24]. Below we provide the flow chart of the conservative SL HWENO with WENO limiters for the VP simulations.

Algorithm 1. Conservative SL HWENO scheme for the VP system.

Step 1. Apply WENO limiter as a pre-processing procedure to reconstruct $\Phi^n_{i+\frac{1}{2},j}$.

First, we use TVB limiter to identify the "troubled cells," namely, those cells which might need the limiting procedure. Let:

$$\tilde{f}_{ij} = \Phi^n_{i+\frac{1}{2},j} - f^n_{ij}, \quad \tilde{\tilde{f}}_{ij} = -\Phi^n_{i-\frac{1}{2},j} + f^n_{ij}. \tag{3.11}$$

These are modified by the modified minmod function;

$$\tilde{f}^{(mod)}_{ij} = \tilde{m}\left(\tilde{f}_{ij}, f^n_{i+1,j} - f^n_{ij}, f^n_{ij} - f^n_{i-1,j}\right), \tag{3.12}$$

$$\tilde{\tilde{f}}^{(mod)}_{ij} = \tilde{m}\left(\tilde{\tilde{f}}_{ij}, f^n_{i+1,j} - f^n_{ij}, f^n_{ij} - f^n_{i-1,j}\right), \tag{3.13}$$

where $\tilde{m}$ is given by

$$\tilde{m}(a_1, a_2, \cdots, a_n) = \begin{cases} a_1 & \text{if } |a_1| \le M_x(\Delta x)^2, \\ m(a_1, a_2, \cdots, a_n) & \text{otherwise}, \end{cases} \tag{3.14}$$

and the minmod function m is given by

$$m(a_1, a_2, \cdots, a_n) = \begin{cases} s \cdot \min_{1 \le j \le n} |a_j| & \text{if } sign(a_1) = sign(a_2) = \cdots = sign(a_n) = s, \\ 0 & \text{otherwise.} \end{cases} \tag{3.15}$$

The TVB limiter parameter $M_x > 0$ is a constant. If $\tilde{f}_{ij}^{(mod)} \neq \tilde{f}_{ij}$ or $\tilde{\tilde{f}}_{ij}^{(mod)} \neq \tilde{\tilde{f}}_{ij}$, we declare the T_{ij} as a troubled cell.

Then we replace $\Phi^n_{i+\frac{1}{2},j}$ and $\Phi^n_{i-\frac{1}{2},j}$ in those troubled cells by WENO reconstruction.

Step 2. Perform a half time step advection in physical space, i.e. the equations in (3.4).

Step 3. Compute the electric field at the half step by substituting f^* into equation (3.2) and solve for $E^*(x)$.

Step 4. Similar to Step 1, we apply WENO limiter as a pre-processing procedure to reconstruct $\Psi^*_{i,j+\frac{1}{2}}$.

Step 5. Perform a full time step advection in velocity space, i.e. the equations in (3.5).

Step 6. We use the same pre-processing procedure like Step 1 to reconstruct $\Phi^{**}_{i+\frac{1}{2},j}$.

Step 7. Perform a half time step advection in physical space.

Remark 3. The proposed scheme for the VP system locally conserves mass due to the flux difference form. In particular, we are working with flux functions Φ and Ψ (but not f_x and f_v). Similar to Proposition 1 for the 1-D case, we have the mass conservation for the 1-D VP system. We skip the proof, as it is similar to that for 1-D as long as we are working with the flux difference form. The time history of mass shown in Fig. 4.11 confirms the mass conservation property of the scheme.

4. Numerical tests

In Section 4.1, we first test a 1-D transport problem, and then the 2-D rigid body rotation via the Strang splitting. In Section 4.2, we test the proposed scheme to classical test problems for VP simulations, such as Landau damping and two-steam instability. In many of the examples in this section, we compare performance of the proposed SL HWENO scheme with the SL WENO scheme in [26].

4.1. Linear test problems

Example 1 *(1-D transport).* Consider the linear advection equation:

$$f_t + f_x = 0, \ x \in [0, 2\pi]. \tag{4.1}$$

The conservative SL methods with fifth order HWENO reconstruction is used to solve equation (4.1). Table 4.1 gives the L_1 error and the corresponding order of convergence of the SL HWENO scheme and SL WENO scheme when applied to equation (4.1) with smooth initial data $f(x, 0) = \sin(x)$. Both methods achieve fifth order accuracy, and error from the SL HWENO scheme is slightly smaller than that from the SL WENO scheme for this example. Next, to evaluate the capability of the scheme in capturing discontinuities and smooth profiles, we consider the following initial distribution with four types of profiles

$$f(x,0) = \begin{cases} \frac{1}{6}(G(x,\beta,z-\delta) + G(x,\beta,z+\delta) + 4G(x,\beta,z)) & \text{for } -0.8 \le x \le -0.6, \\ 1 & \text{for } -0.4 \le x \le -0.2, \\ 1 - |10(x-0.1)| & \text{for } 0.0 \le x \le 0.2, \\ \frac{1}{6}(F(x,\alpha,a-\delta) + F(x,\alpha,a+\delta) + 4F(x,\alpha,a)) & \text{for } 0.4 \le x \le 0.6, \\ 0 & \text{otherwise,} \end{cases} \tag{4.2}$$

where $G(x,\beta,z) = e^{-\beta(x-z)^2}$ and $F(x,\alpha,a) = \sqrt{\max(1-\alpha^2(x-a)^2, 0)}$. The constants are specified as $a = 0.5, z = -0.7, \delta = 0.005, \alpha = 10$ and $\beta = \frac{\log 2}{36\delta^2}$. The boundary condition is periodic. We compute the solution up to $t = 8$ with 200 points. The result is shown in Fig. 4.1. Non-oscillatory numerical capture of discontinuities is observed.

Table 4.1
Order of accuracy for (4.1) with $f(x, t = 0) = \sin(x)$ at $T = 20$. $CFL = 1.2$.

N	HWENO		WENO	
	L_1 error	Order	L_1 error	Order
32	4.03E−05	–	7.31E−05	–
64	1.17E−06	5.10	2.23E−06	5.03
96	1.52E−07	5.05	2.93E−07	5.00
128	3.56E−08	5.04	6.97E−08	5.00
160	1.16E−08	5.03	2.28E−08	5.00
192	4.62E−09	5.03	9.16E−09	5.00

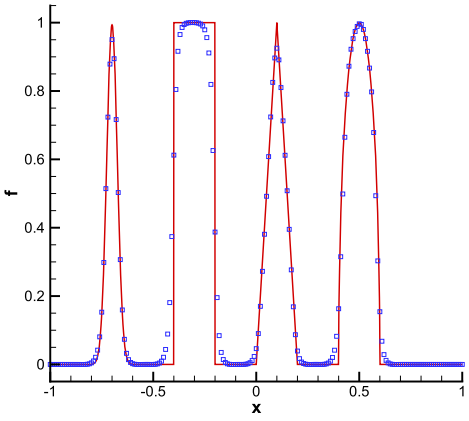

Fig. 4.1. The SL HWENO scheme; 200 points, $CFL = 1.2$, $T = 8$.

Table 4.2
Order of accuracy for (4.3) with $f(x, y, t = 0) = \exp(-x^2 - y^2)$ at $T = 2\pi$. $CFL = 1.2$.

N	L_1 error	Order	L_2 error	Order	L_∞ error	Order
20	1.31E−02		2.49E−02		1.19E−01	
40	1.05E−03	3.65	1.90E−03	3.71	1.50E−02	2.99
80	4.34E−05	4.59	8.88E−05	4.42	4.99E−04	4.91
160	2.03E−06	4.42	3.97E−06	4.48	2.11E−05	4.56
320	6.50E−08	4.96	1.36E−07	4.87	7.33E−07	4.85

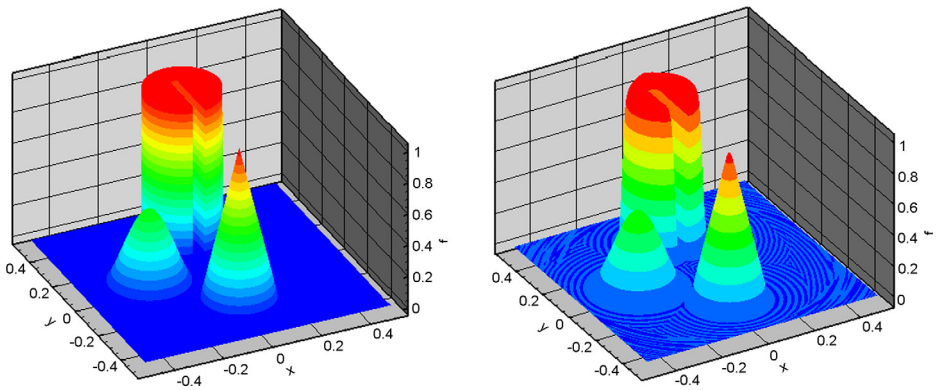

(a) The initial profile (b) SLHWENO with $CFL = 1.2$

Fig. 4.2. Left: Plots of the initial profile. Right: Plots of the numerical solution for equation (4.4); $CFL = 1.2$; $T = 1$; The numerical mesh has a resolution of 200×200; Conservative SL HWENO scheme without WENO limiter. (For interpretation of the colors in this figure, the reader is referred to the web version of this article.)

Example 2 *(Rigid body rotation).* Consider the rigid body rotation

$$f_t - yf_x + xf_y = 0, \quad \text{on} \quad [-2\pi, 2\pi] \times [-2\pi, 2\pi]. \tag{4.3}$$

First, we consider a smooth initial condition $f(x, y, 0) = \exp(-x^2 - y^2)$ for accuracy test. Table 4.2 gives the error and convergence rates of the scheme for the time step $\Delta t = CFL/(\frac{2\pi}{\Delta x} + \frac{2\pi}{\Delta y})$ with $CFL = 1.2$ for smooth initial data. The high order convergence of the scheme is observed.

Secondly, we consider a test case introduced in [20],

$$f_t - 2\pi yf_x + 2\pi xf_y = 0, \quad \text{on} \quad [-0.5, 0.5] \times [-0.5, 0.5], \tag{4.4}$$

with an initial condition containing a slotted disk, a cone and a smooth hump, as plotted in Fig. 4.2. The numerical solution after one full revolution by the conservative SL HWENO scheme (denoted as CSLHWENO-WO) is plotted in Fig. 4.2. The time step $\Delta t = CFL/(\frac{\pi}{\Delta x} + \frac{\pi}{\Delta y})$ with $CFL = 1.2$. When we increase the CFL to be 2.2, the solution of the scheme without WENO limiter will be oscillatory. We apply the WENO limiter to the scheme (denoted as CSLHWENO-WL). The numerical solution

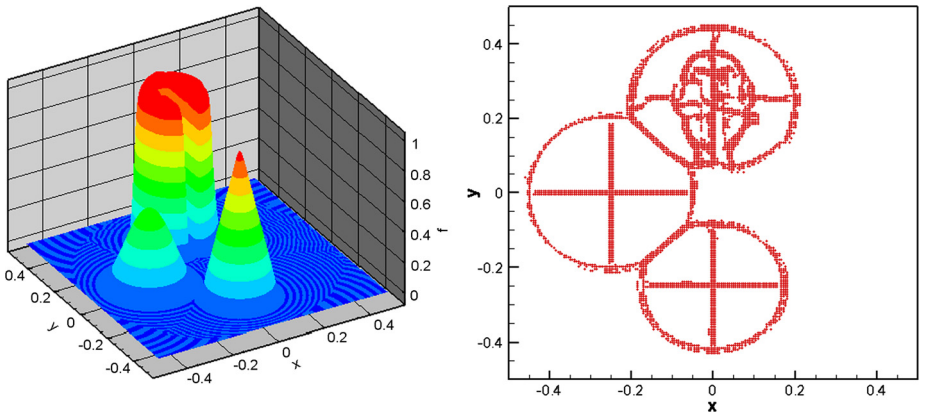

Fig. 4.3. Left: The numerical solution for equation (4.4). Right: Trouble cells. $CFL = 2.2$. TVB constant $M = 1.0$. $T = 1$. The numerical mesh has a resolution of 200×200. Conservative SL HWENO scheme with WENO limiter. (For interpretation of the colors in this figure, the reader is referred to the web version of this article.)

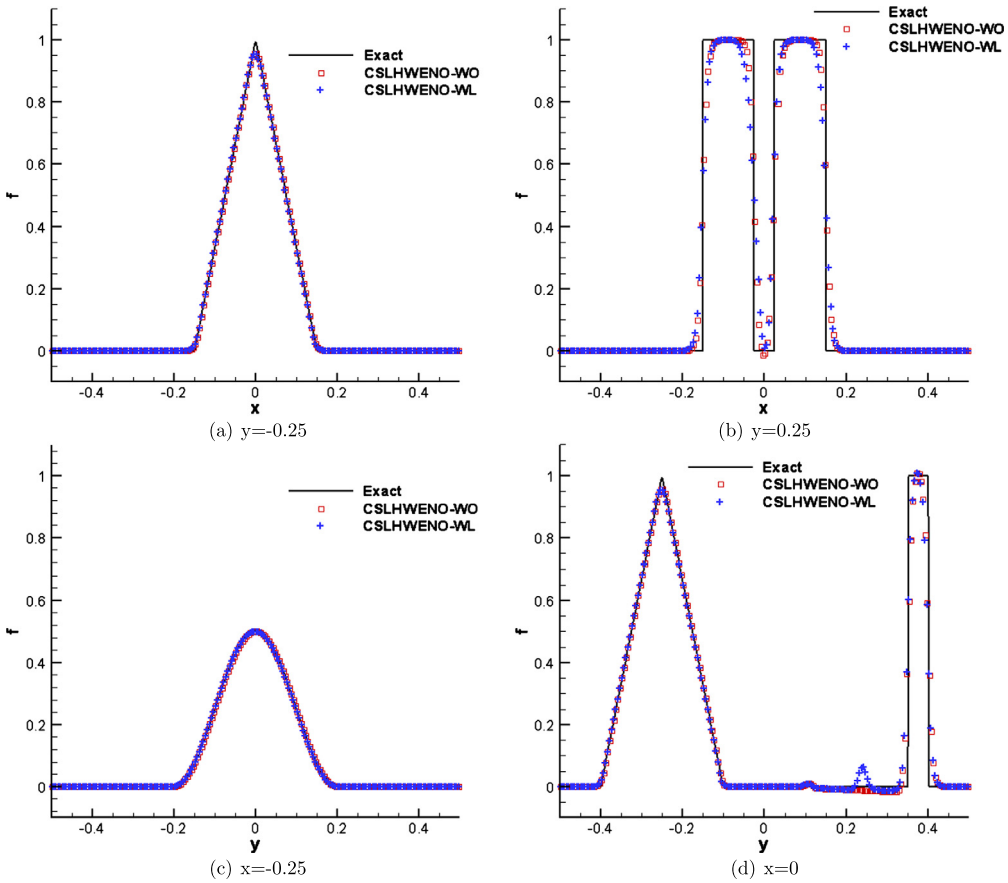

Fig. 4.4. Plots of the 1-D cuts of the numerical solution for equation (4.4) at $y = -0.25, y = 0.25, x = -0.25, x = 0$ (from top left to bottom right). The solid line depicts the exact solution. The numerical mesh has a resolution of 200×200.

and trouble cells at the last time step are presented in Fig. 4.3. In Fig. 4.4, we plot the 1-D cut of the solution compared with the exact solution. Non-oscillatory capturing of discontinuities is observed.

4.2. The VP system

In this subsection, we apply the conservative SL HWENO scheme to the VP system. Periodic boundary conditions are imposed in the x-direction and zero boundary conditions are imposed in the v-direction for all of our test problems.

Table 4.3
Order of accuracy in space for the SL HWENO scheme and the SL WENO scheme: two stream instability. $T = 0.2$ and $CFL = 0.01$.

$N_x \times N_v$	HWENO		WENO	
	L_1 error	Order	L_1 error	Order
16×16	2.65E−04	–	2.74E−04	–
32×32	2.52E−05	3.39	3.08E−05	3.15
48×48	2.59E−06	5.62	5.63E−06	4.19
64×64	6.07E−07	5.04	1.52E−06	4.55
80×80	2.05E−07	4.86	5.29E−07	4.73

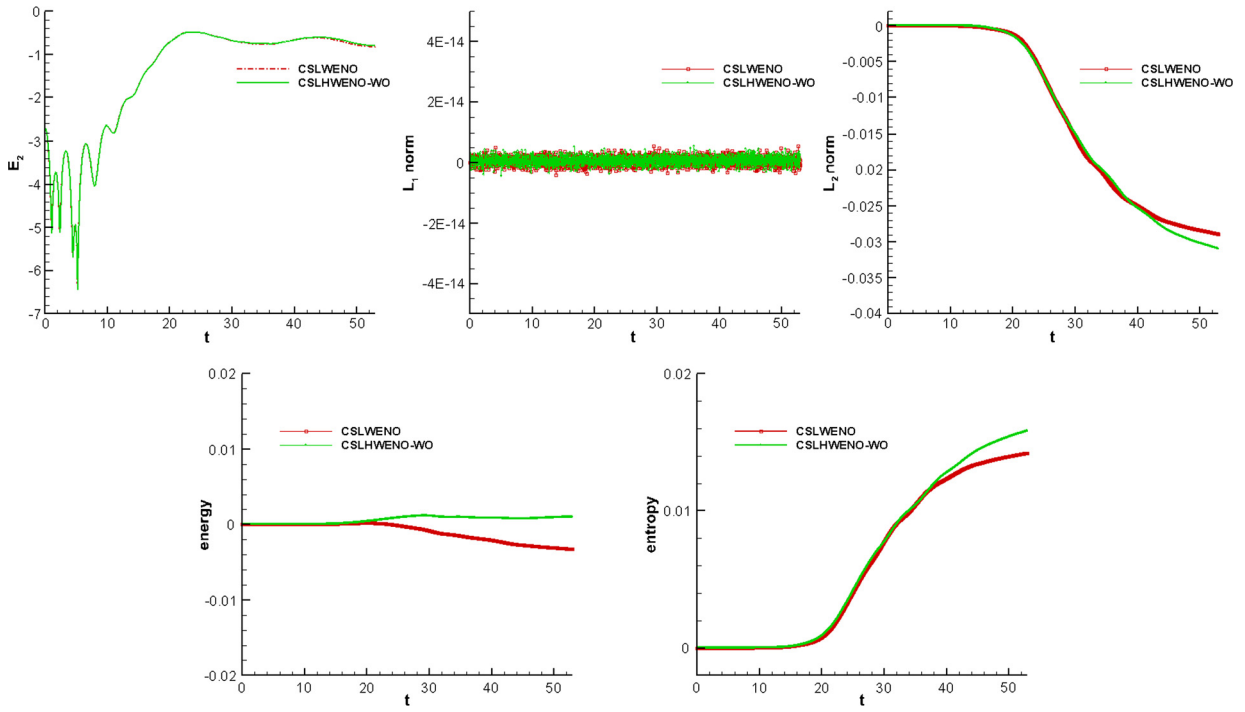

Fig. 4.5. Two-stream instability: time evolution of the electric field in L^2 (upper left), time evolution of the relative deviations of L^1 (upper middle) and L^2 (upper right) norms of the solution as well as the discrete kinetic energy (lower left) and entropy (lower right) for CSLWENO and CSLHWENO-WO.

Because of the periodicity in space, a fast Fourier transform (FFT) is used to solve the 1-D Poisson equation. $\rho(x,t)$ is computed by the rectangular rule, $\rho(x,t) = \int f(x,v,t)dv = \sum_j f(x,v_j,t)\Delta v$, which is spectrally accurate [6], when the underlying function is smooth enough. We recall several norms in the VP system below, which remain constant in time.

1. L^p norm $1 \le p \le \infty$:

$$\|f\|_p = \left(\int_v \int_x |f(x,v,t)|^p dxdv \right)^{\frac{1}{p}}. \tag{4.5}$$

2. Energy:

$$Energy = \int_v \int_x f(x,v,t)v^2 dxdv + \int_x E^2(x,t)dx, \tag{4.6}$$

where $E(x,t)$ is the electric field.

3. Entropy:

$$Entropy = \int_v \int_x f(x,v,t)\log(f(x,v,t))dxdv. \tag{4.7}$$

Tracking relative deviations of these quantities numerically will be a good measurement of the quality of numerical schemes. The relative deviation is defined to be the deviation away from the corresponding initial value divided by the magnitude

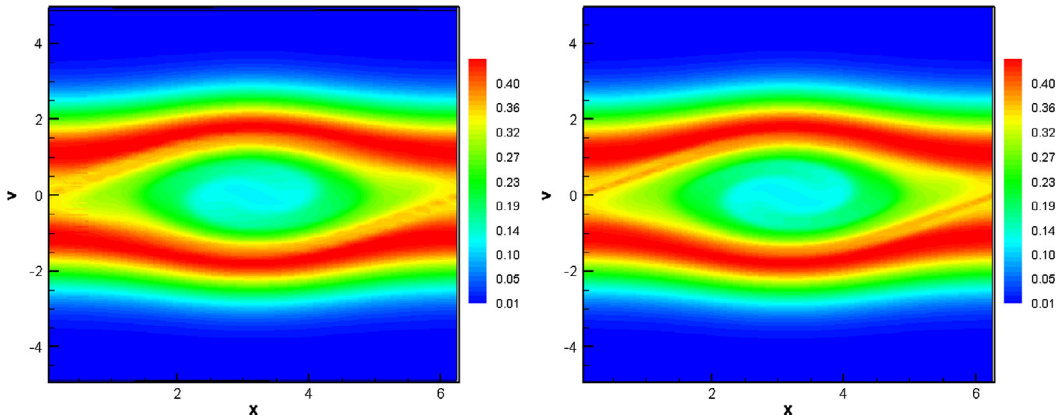

(a) CSLWENO (b) CSLHWENO-WO

Fig. 4.6. Phase space plots of the two stream instability at $T = 53$. The numerical mesh is 64×128. Left: CSLWENO. Right: CSLHWENO-WO ($CFL = 1.2$). (For interpretation of the colors in this figure, the reader is referred to the web version of this article.)

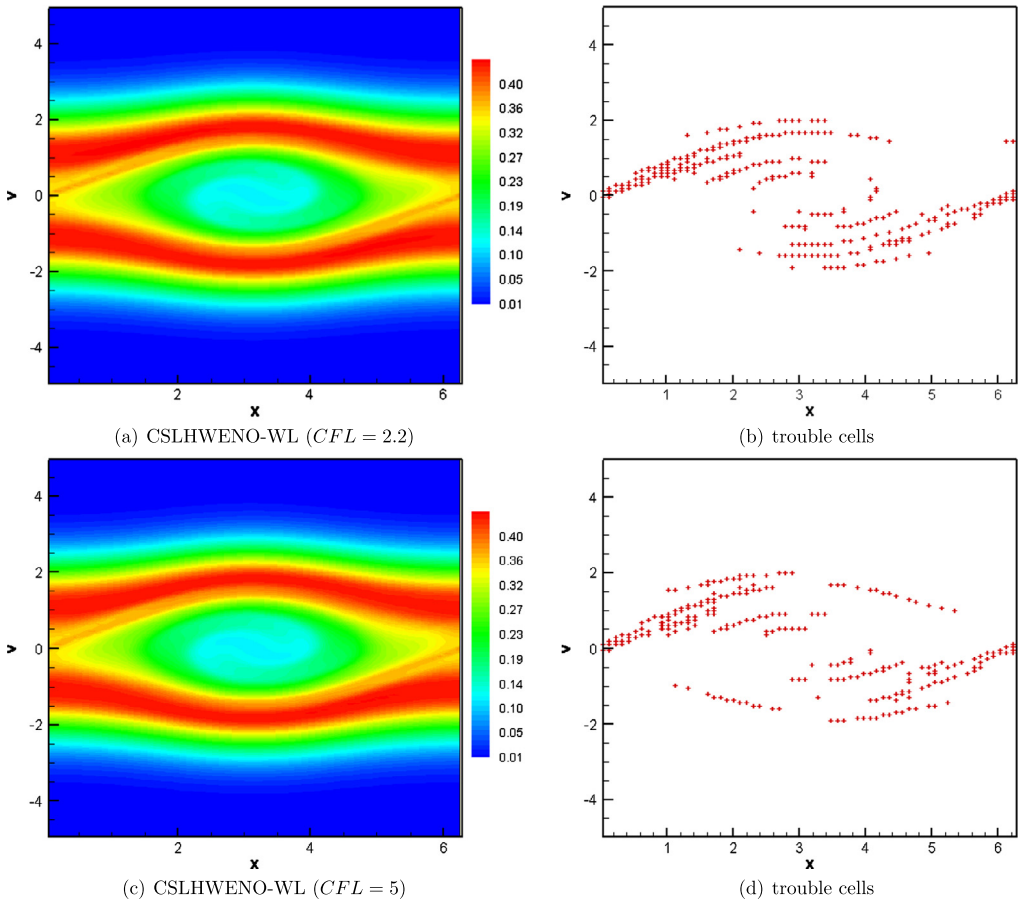

(a) CSLHWENO-WL ($CFL = 2.2$) (b) trouble cells

(c) CSLHWENO-WL ($CFL = 5$) (d) trouble cells

Fig. 4.7. Phase space plots of the two stream instability at $T = 53$. The numerical mesh is 64×128. Top left: CSLHWENO-WL ($CFL = 2.2$); the TVB constants $M_x = 1, M_y = 1$. Top right: trouble cells of CSLHWENO-WL ($CFL = 2.2$) at the last time step. Bottom left: CSLHWENO-WL ($CFL = 5$); the TVB constants $M_x = 1, M_y = 1$. Bottom right: trouble cells of CSLHWENO-WL ($CFL = 5$) at the last time step. (For interpretation of the colors in this figure, the reader is referred to the web version of this article.)

of the initial value. It is expected that our scheme will conserve mass. However, the positivity of f will not be preserved. Thus, when numerically computing the entropy, we compute $\int_v \int_x f(x, v, t) \log |f(x, v, t)| dxdv$. We set the time step by $\Delta t = CFL/(v_{max}/\Delta x + \max(E(x))/\Delta v)$, where v_{max} is the maximum velocity on the phase space mesh with CFL specified in our description below.

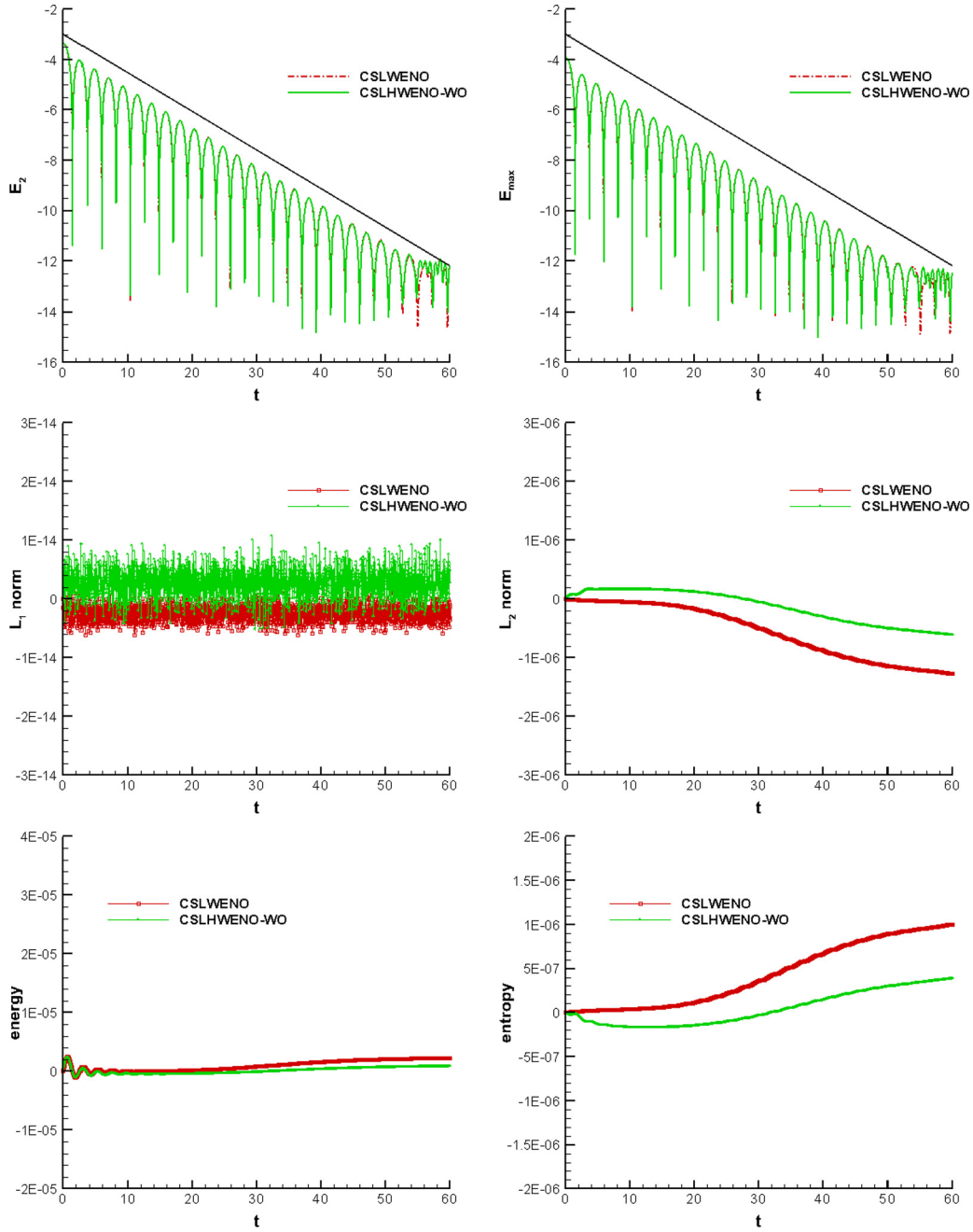

Fig. 4.8. Weak Landau damping: time evolution of the electric field in L^2 (upper left) and L^∞ (upper right) norms, time evolution of the relative deviations of L^1 (middle left) and L^2 (middle right) norms of the solution as well as the discrete kinetic energy (lower left) and entropy (lower right).

We first test the conservative SL HWENO scheme with $CFL = 1.2$, denoted as "CSLHWENO-WO", to solve the VP system. This schemes will be compared with the fifth order conservative SL WENO scheme proposed in [26] with the same $CFL = 1.2$, denoted as "CSLWENO". Moreover, we will study the conservative SL HWENO scheme with the larger CFL. For example, if $CFL = 2.2$, the WENO limiter in certain TVB constants is needed to enforce the stability of this scheme, and denote the scheme as "CSLHWENO-WL($CFL = 2.2$)".

Example 3 *(Two stream instability [13]).* Consider two stream instability, with the initial distribution function,

$$f(x, v, t = 0) = \frac{2}{7\sqrt{2\pi}}(1 + 5v^2)(1 + \alpha\,((\cos(2kx) + \cos(3kx))/1.2 + \cos(kx)))\exp\left(-\frac{v^2}{2}\right)$$

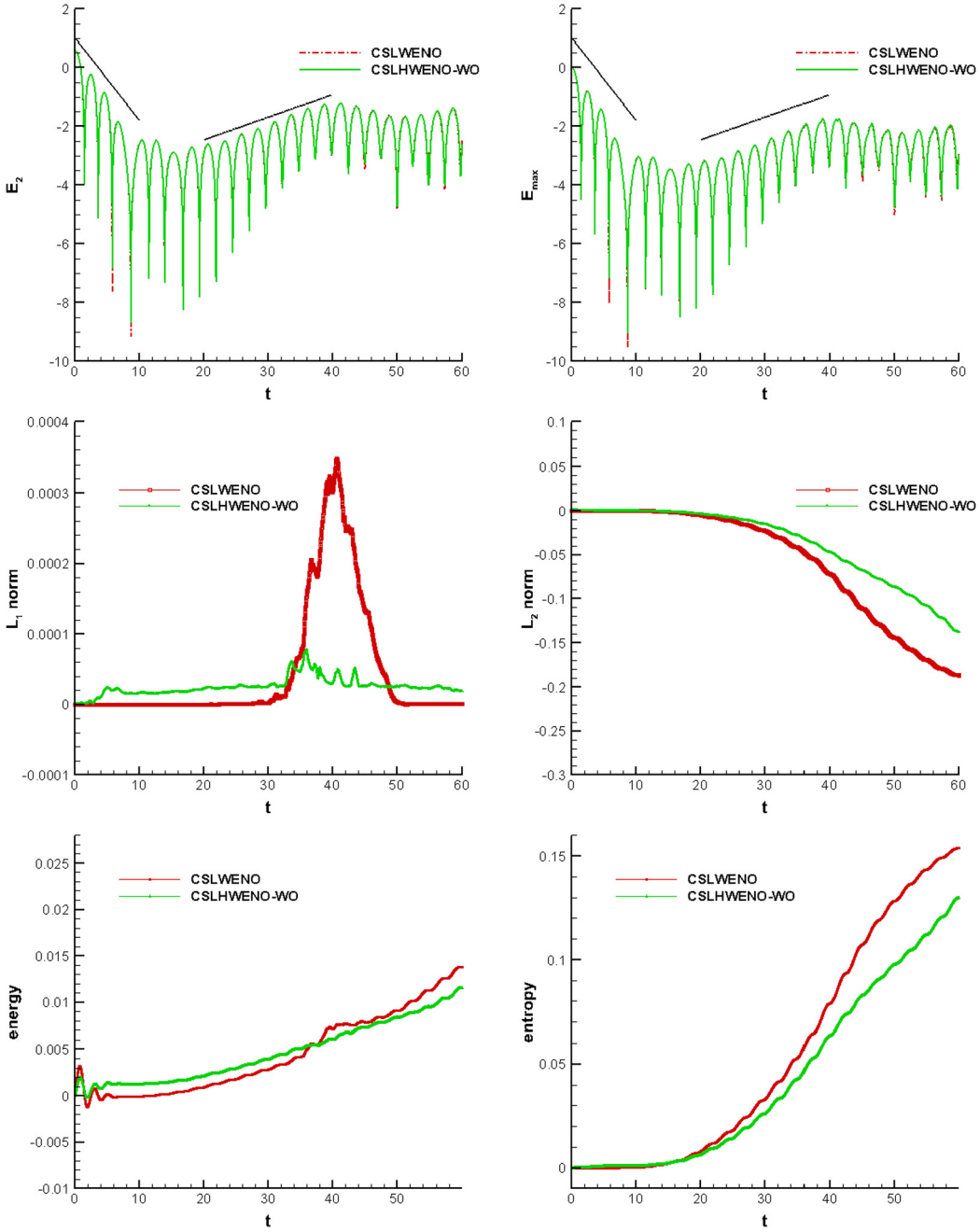

Fig. 4.9. Strong Landau damping: time evolution of the electric field in L^2 (upper left) and L^∞ (upper right) norms, time evolution of the relative deviations of L^1 (middle left) and L^2 (middle right) norms of the solution as well as the discrete kinetic energy (lower left) and entropy (lower right).

where $\alpha = 0.01,\ k = 0.5$. The length of the domain in the x direction is $L = \frac{2\pi}{k}$ and the background ion distribution function is fixed, uniform and chosen so that the total net charge density for the system is zero.

We first test the spatial accuracy of the conservative SL HWENO scheme. We set $CFL = 0.01$ so that the spatial error is the dominant error. In Table 4.3, we observe that both the SL HWENO scheme and the SL WENO scheme have fifth order accuracy, and the SL HWENO scheme is more accurate than the SL WENO scheme. Then we test the reliability of the two methods after a long time integration with $v_{max} = 5$, $N_x = 64$, $N_v = 128$. In Fig. 4.5, the time evolution of the L^2 norm of the electric field (in semi-log scale), the discrete L^1 norm, L^2 norm, kinetic energy and entropy are plotted. Comparable results are observed. In Fig. 4.6, we show numerical solutions at $T = 53$ of CSLWENO, CSLHWENO-WO at $CFL = 1.2$. The scheme with HWENO seems to have slightly better resolution of the solution. In Fig. 4.7, we show numerical solutions, as

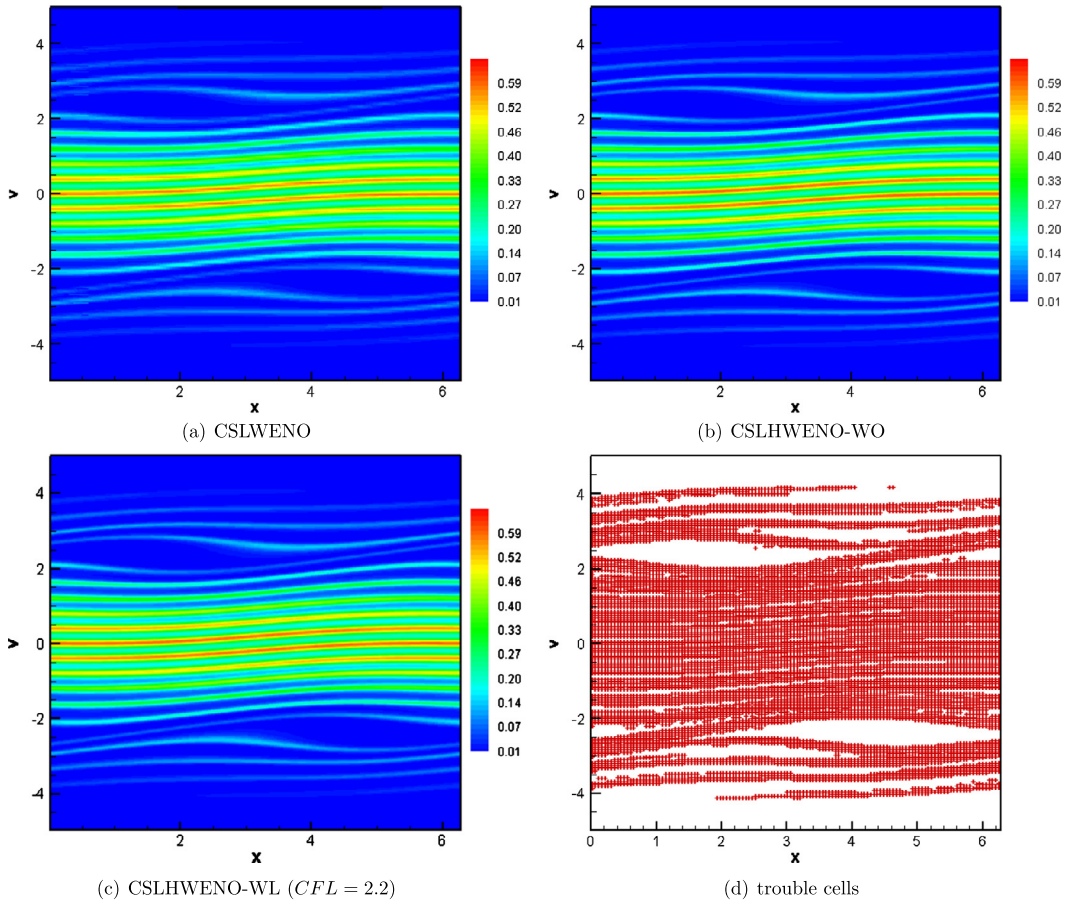

Fig. 4.10. Strong Landau damping. $T = 30$. $N_x \times N_v = 128 \times 256$. Top left: CSLWENO. Top right: CSLHWENO-WO ($CFL = 1.2$). Bottom left: CSLHWENO-WL ($CFL = 2.2$); the TVB constants $M_x = M_y = 1$. Bottom right: trouble cells of CSLHWENO-WL ($CFL = 2.2$) at the last time step. (For interpretation of the colors in this figure, the reader is referred to the web version of this article.)

well as trouble cells identified in the last time step, from the scheme with larger CFLs (2.2 and 5) and with the WENO limiter. Note that the solution of CSLHWENO-WO at $CFL = 2.2$ will be oscillatory without the limiter (not presented here).

Example 4 *(Weak Landau damping).* Consider the weak Landau damping for the VP system. The initial condition used here is,

$$f(x, v, t = 0) = \frac{1}{\sqrt{2\pi}}(1 + \alpha \cos(kx)) \exp\left(-\frac{v^2}{2}\right), \tag{4.8}$$

with $\alpha = 0.01$ and $k = 0.5$. Our simulation parameters are $v_{max} = 5$, $N_x = 64$, $N_v = 128$. The time evolution of the L^2 and L^∞ norms of the electric field (in semi-log scale) are plotted in the upper plots of Fig. 4.8. The correct damping of the electric field of CSLWENO and CSLHWENO-WO is observed in the plots, benchmarked with the theoretical value $\gamma = 0.1533$ [14] (the solid line in the same plots). We observe that the conservative SL scheme generates very consistent results, performing very well in recovering the damping rate. Time evolution of the relative deviations of the L^1, L^2 solution norms, energy, entropy in the discrete sense are demonstrated in the middle and bottom plots in Fig. 4.8. The advantage of using conservative schemes in preserving the relevant physical norms is observed. CSLHWENO-WO is observed to perform slightly better than the CSLWENO in preserving norms.

Example 5 *(Strong Landau damping).* Consider the strong Landau damping for the VP system. We simulate the VP system with the initial condition in equation (4.8) with $\alpha = 0.5$ and $k = 0.5$. Our simulation parameters are $v_{max} = 5$, $N_x = 128$, $N_v = 256$. In the first row of Fig. 4.9, the time evolution of the L^2 and L^∞ norms of the electric field with the linear decay rate $\gamma_1 = -0.2812$ and $\gamma_2 = 0.0770$ [7,16] (in semi-log scale) are plotted. The time evolution of the relative deviations of discrete L^1 norm, L^2 norm, kinetic energy and entropy for CSLWENO and CSLHWENO-WO are plotted in the second and third rows of Fig. 4.9. CSLHWENO-WO scheme is observed to perform slightly better in preserving these norms than the CSLWENO scheme. In Fig. 4.10, numerical solutions of CSLWENO and CSLHWENO-WO at $t = 30$ are plotted. Compared with

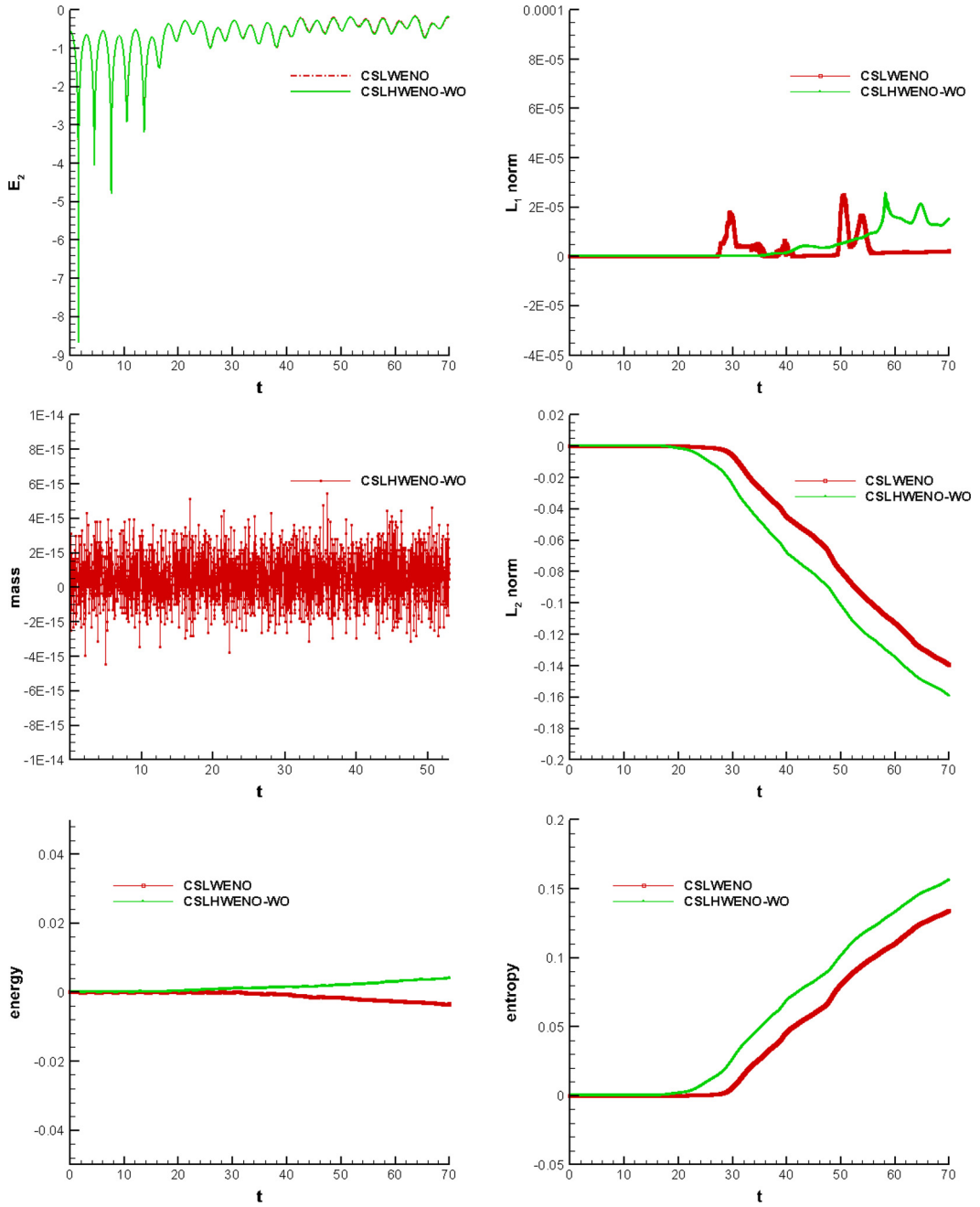

Fig. 4.11. Two-stream instability: time evolution of the electric field in L^2 (upper left) and L^∞ (upper right) norms, L^1 (middle left) and L^2 (middle right) norms of the solution as well as the discrete kinetic energy (lower left) and entropy (lower right).

CSLWENO, slightly better resolution is observed for CSLHWENO-WO. The solution profile of the conservative SL HWENO scheme with $CFL = 2.2$ and with WENO limiter, as well as the trouble cells identified in the last step, are presented in the bottom plots of Fig. 4.10. Comparable solution profiles are observed.

Example 6 *(Two stream instability [32,10]).* Consider the symmetric two stream instability,

$$f(x, v, t = 0) = \frac{1}{2v_{th}\sqrt{2\pi}}\left[\exp\left(-\frac{(v-u)^2}{2v_{th}^2}\right) + \exp\left(-\frac{v+u}{2v_{th}^2}\right)\right](1 + 0.05\cos(kx))$$

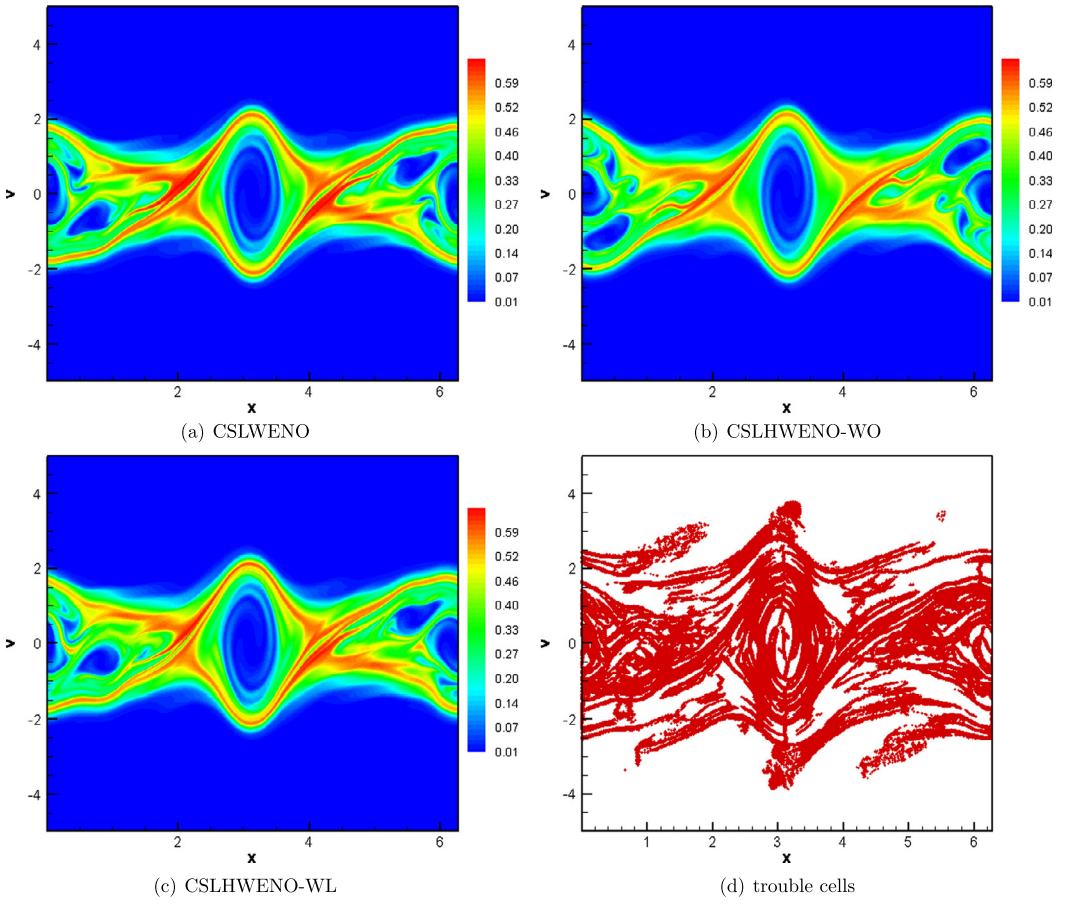

Fig. 4.12. Phase space plots of the two stream instability at $T = 70$. The numerical mesh is 512×512. Top left: CSLWENO. Top right: CSLHWENO-WO ($CFL = 1.2$). Bottom left: CSLHWENO-WL ($CFL = 2.2$). Bottom right: trouble cells of CSLHWENO-WL at the last time step. (For interpretation of the colors in this figure, the reader is referred to the web version of this article.)

with $u = 0.99$, $v_{th} = 0.3$ and $k = \frac{2}{13}$. Our numerical simulation parameters are $v_{max} = 5$, $N_x = 512$, $N_v = 512$. In the upper left plot of Fig. 4.11, the time evolution of the L^2 norm of the electric field (in semi-log scale) for CSLWENO and CSLHWENO-WO is plotted. Then the discrete L^1 norm ($\int_v \int_x |f| dxdv$), mass ($\int_v \int_x f dxdv$), L^2 norm, energy and entropy of both schemes are plotted. Comparable results are observed. It is observed that the mass is being preserved, but not the L^1 norm as our numerical solution does not enjoy positivity preserving property. Fig. 4.12 shows numerical solutions of phase space profiles for CSLWENO, CSLHWENO-WO and CSLHWENO-WL ($CFL = 2.2$) at $T = 70$. The TVB constants of CSLHWENO-WL ($CFL = 2.2$) are $M_x = M_y = 0.1$.

5. Conclusions

In this paper, we propose a conservative SL HWENO scheme for VP system based on dimensional splitting. Compared with the original WENO reconstruction, the advantage of HWENO reconstruction is compact. To ensure local mass conservation, the derivative in the scheme is rewritten as the flux-difference form. The fifth order conservative SL HWENO scheme for the flux difference is proposed. The scheme can be extended to solve high dimensional problem by the Strang splitting method. We show the SL HWENO scheme with the Eulerian CFL condition perform well for the classical Landau damping and the two-steam instability in plasma physics. When the time stepping size is larger than the Eulerian CFL restriction, we introduce WENO limiters to control oscillations.

References

[1] B. Ayuso, J.A. Carrillo, C.-W. Shu, Discontinuous Galerkin methods for the one-dimensional Vlasov–Poisson system, Kinet. Relat. Models 4 (2011) 955–989.
[2] D. Barnes, T. Kamimura, J.-N. Leboeuf, T. Tajima, Implicit particle simulation of magnetized plasmas, J. Comput. Phys. 52 (1983) 480–502.
[3] J. Barnes, P. Hut, A hierarchical $o(N \log N)$ force-calculation algorithm, Nature 324 (6096) (1986) 446–449.
[4] N. Besse, Convergence of a high-order semi-Lagrangian scheme with propagation of gradients for the one-dimensional Vlasov–Poisson system, SIAM J. Numer. Anal. 46 (2008) 639–670.

[5] N. Besse, E. Sonnendrücker, Semi-Lagrangian schemes for the Vlasov equation on an unstructured mesh of phase space, J. Comput. Phys. 191 (2003) 341–376.
[6] J.P. Boyd, Chebyshev and Fourier Spectral Methods, Courier Corporation, 2001.
[7] C.-Z. Cheng, G. Knorr, The integration of the Vlasov equation in configuration space, J. Comput. Phys. 22 (1976) 330–351.
[8] Y. Cheng, I.M. Gamba, P.J. Morrison, Study of conservation and recurrence of Runge–Kutta discontinuous Galerkin schemes for Vlasov–Poisson systems, J. Sci. Comput. 56 (2013) 319–349.
[9] B. Cockburn, C.-W. Shu, Runge–Kutta discontinuous Galerkin methods for convection-dominated problems, J. Sci. Comput. 16 (2001) 173–261.
[10] N. Crouseilles, M. Mehrenberger, E. Sonnendrücker, Conservative semi-Lagrangian schemes for Vlasov equations, J. Comput. Phys. 229 (2010) 1927–1953.
[11] B.A. de Dios, J.A. Carrillo, C.-W. Shu, Discontinuous Galerkin methods for the multi-dimensional Vlasov–Poisson problem, Math. Models Methods Appl. Sci. 22 (2012) 1250042.
[12] E. Evstatiev, B. Shadwick, Variational formulation of particle algorithms for kinetic plasma simulations, J. Comput. Phys. 245 (2013) 376–398.
[13] F. Filbet, E. Sonnendrücker, Comparison of Eulerian Vlasov solvers, Comput. Phys. Commun. 150 (2003) 247–266.
[14] F. Filbet, E. Sonnendrücker, P. Bertrand, Conservative numerical schemes for the Vlasov equation, J. Comput. Phys. 172 (2001) 166–187.
[15] A. Friedman, S. Parker, S. Ray, C. Birdsall, Multi-scale particle-in-cell plasma simulation, J. Comput. Phys. 96 (1991) 54–70.
[16] W. Guo, J.-M. Qiu, Hybrid semi-Lagrangian finite element-finite difference methods for the Vlasov equation, J. Comput. Phys. 234 (2013) 108–132.
[17] R. Heath, I.M. Gamba, P.J. Morrison, C. Michler, A discontinuous Galerkin method for the Vlasov–Poisson system, J. Comput. Phys. 231 (2012) 1140–1174.
[18] G. Jacobs, J.S. Hesthaven, High-order nodal discontinuous Galerkin particle-in-cell method on unstructured grids, J. Comput. Phys. 214 (2006) 96–121.
[19] G.-S. Jiang, C.-W. Shu, Efficient implementation of weighted ENO schemes, J. Comput. Phys. 126 (1996) 202–228.
[20] R. LeVeque, High-resolution conservative algorithms for advection in incompressible flow, SIAM J. Numer. Anal. (1996) 627–665.
[21] H. Liu, J. Qiu, Finite difference Hermite WENO schemes for hyperbolic conservation laws, J. Sci. Comput. 63 (2015) 548–572.
[22] T. Nakamura, T. Yabe, Cubic interpolated propagation scheme for solving the hyper-dimensional Vlasov—Poisson equation in phase space, Comput. Phys. Commun. 120 (1999) 122–154.
[23] J. Qiu, C.-W. Shu, Hermite WENO schemes and their application as limiters for Runge–Kutta discontinuous Galerkin method: one-dimensional case, J. Comput. Phys. 193 (2004) 115–135.
[24] J. Qiu, C.-W. Shu, Runge–Kutta discontinuous Galerkin method using WENO limiters, SIAM J. Sci. Comput. 26 (2005) 907–929.
[25] J.-M. Qiu, A. Christlieb, A conservative high order semi-Lagrangian WENO method for the Vlasov equation, J. Comput. Phys. 229 (2010) 1130–1149.
[26] J.-M. Qiu, C.-W. Shu, Conservative high order semi-Lagrangian finite difference WENO methods for advection in incompressible flow, J. Comput. Phys. 230 (2011) 863–889.
[27] J.-M. Qiu, C.-W. Shu, Conservative semi-Lagrangian finite difference WENO formulations with applications to the Vlasov equation, Commun. Comput. Phys. 10 (2011) 979–1000.
[28] J.-M. Qiu, C.-W. Shu, Positivity preserving semi-Lagrangian discontinuous Galerkin formulation: theoretical analysis and application to the Vlasov–Poisson system, J. Comput. Phys. 230 (2011) 8386–8409.
[29] J.A. Rossmanith, D.C. Seal, A positivity-preserving high-order semi-Lagrangian discontinuous Galerkin scheme for the Vlasov–Poisson equations, J. Comput. Phys. 230 (2011) 6203–6232.
[30] C.-W. Shu, S. Osher, Efficient implementation of essentially non-oscillatory shock-capturing schemes, II, J. Comput. Phys. 83 (1989) 32–78.
[31] E. Sonnendrücker, J. Roche, P. Bertrand, A. Ghizzo, The semi-Lagrangian method for the numerical resolution of the Vlasov equation, J. Comput. Phys. 149 (1999) 201–220.
[32] T. Umeda, A conservative and non-oscillatory scheme for Vlasov code simulations, Earth Planets Space 60 (2008) 773–779.
[33] T. Xiong, J.-M. Qiu, Z. Xu, A. Christlieb, High order maximum principle preserving semi-Lagrangian finite difference WENO schemes for the Vlasov equation, J. Comput. Phys. 273 (2014) 618–639.
[34] C. Yang, F. Filbet, Conservative and non-conservative methods based on Hermite weighted essentially non-oscillatory reconstruction for Vlasov equations, J. Comput. Phys. 279 (2014) 18–36.
[35] S. Zaki, T. Boyd, L. Gardner, A finite element code for the simulation of one-dimensional Vlasov plasmas. II. Applications, J. Comput. Phys. 79 (1988) 200–208.
[36] S. Zaki, L. Gardner, T. Boyd, A finite element code for the simulation of one-dimensional Vlasov plasmas. I. Theory, J. Comput. Phys. 79 (1988) 184–199.
[37] T. Zhou, Y. Guo, C.-W. Shu, Numerical study on Landau damping, Phys. D, Nonlinear Phenom. 157 (2001) 322–333.
[38] J. Zhu, J. Qiu, A class of the fourth order finite volume Hermite weighted essentially non-oscillatory schemes, Sci. China Ser. A, Math. 51 (2008) 1549–1560.